

An Isomer Study of the Nucleus  $^{54}\text{Ni}$   
Preparations, Simulations,  
and First Results

MASTER OF SCIENCE THESIS

Robert Hoischen

Supervisor: Dr. Dirk Rudolph



**LUNDS**  
UNIVERSITET

DEPARTMENT OF PHYSICS  
NUCLEAR STRUCTURE GROUP  
LUND UNIVERSITY  
2006



# Contents

|          |   |           |
|----------|---|-----------|
| <b>1</b> | <b>Introduction</b>                               | <b>5</b>  |
| <b>2</b> | <b>Physical Background</b>                        | <b>7</b>  |
| 2.1      | Mirror Nuclei . . . . .                           | 7         |
| 2.2      | Isomeric States . . . . .                         | 8         |
| 2.3      | Branching Ratios . . . . .                        | 8         |
| <b>3</b> | <b>The RISING Stopped Beam Campaign</b>           | <b>9</b>  |
| 3.1      | Intent . . . . .                                  | 9         |
| 3.2      | Experimental Method: Fragmentation . . . . .      | 9         |
| 3.3      | $^{54}\text{Ni}$ Experiment . . . . .             | 10        |
| <b>4</b> | <b>Experimental Setup</b>                         | <b>13</b> |
| 4.1      | The FRS . . . . .                                 | 13        |
| 4.1.1    | Function and Concept . . . . .                    | 14        |
| 4.1.2    | Ion-Optics . . . . .                              | 14        |
| 4.1.3    | Component Overview . . . . .                      | 15        |
| 4.1.4    | A special component: the Wedge Degradar . . . . . | 15        |
| 4.2      | Particle Identification . . . . .                 | 16        |
| 4.2.1    | Scintillation Detectors . . . . .                 | 16        |
| 4.2.2    | Multiwires . . . . .                              | 18        |
| 4.2.3    | MUSIC . . . . .                                   | 18        |
| 4.3      | Stopper and Implantation . . . . .                | 18        |
| 4.4      | Ge-Detectors . . . . .                            | 19        |
| <b>5</b> | <b>Simulations</b>                                | <b>21</b> |
| 5.1      | MOCADI . . . . .                                  | 22        |
| 5.2      | Implementation . . . . .                          | 22        |
| 5.2.1    | Initialisation . . . . .                          | 23        |
| 5.2.2    | The Beam, Target and Fragment Card . . . . .      | 24        |
| 5.2.3    | Implementation of Ion Optics and Slits . . . . .  | 25        |
| 5.2.4    | Matter, Wedge Degradar and Implantation . . . . . | 28        |
| 5.2.5    | Time of Flight . . . . .                          | 30        |
| 5.2.6    | Saving . . . . .                                  | 31        |
| 5.2.7    | Finishing the Simulation . . . . .                | 32        |
| 5.3      | Output Files . . . . .                            | 33        |

|           |   |           |
|-----------|---|-----------|
| 5.4       | A MOCADI How-To . . . . .                               | 35        |
| 5.4.1     | Getting Started . . . . .                               | 35        |
| 5.4.2     | Calibrating the Optics and Eliminating Errors . . . . . | 37        |
| 5.4.3     | Important Parameters for the Experiment . . . . .       | 38        |
| 5.5       | LISE++ . . . . .  | 39        |
| 5.5.1     | Building a Simulation . . . . .                         | 39        |
| 5.5.2     | Creating a Setting . . . . .                            | 39        |
| 5.5.3     | Running a Simulation and Plotting the Results . . . . . | 40        |
| <b>6</b>  | <b>Results</b>  | <b>41</b> |
| 6.1       | Calibration Settings . . . . .                          | 41        |
| 6.2       | $^{54}\text{Fe}$ Setting . . . . .                      | 42        |
| 6.3       | $^{54}\text{Ni}$ Setting . . . . .                      | 43        |
| 6.4       | $^{43}\text{V}$ Setting . . . . .                       | 46        |
| <b>7</b>  | <b>The Experiment</b>                                   | <b>47</b> |
| 7.1       | Calibrations . . . . .                                  | 47        |
| 7.2       | Data-Run Summary . . . . .                              | 49        |
| <b>8</b>  | <b>Preliminary Data Analysis</b>                        | <b>51</b> |
| 8.1       | Concept . . . . .                                       | 51        |
| 8.2       | Discussion . . . . .                                    | 58        |
| <b>9</b>  | <b>Conclusions and Outlook</b>                          | <b>63</b> |
| <b>10</b> | <b>Populärvetenskaplig Sammanfattning</b>               | <b>65</b> |
| <b>11</b> | <b>Acknowledgments</b>                                  | <b>67</b> |
|           | <b>Bibliography</b>                                     | <b>67</b> |

# Chapter 1

## Introduction

Our understanding of nuclear physics in general has led to major advances in many areas, for example within medical and environmental technologies, energy production and material sciences. Experiments in nuclear structure physics have the goal to probe the behaviour and structure of nuclear matter in the form of atomic nuclei. Theoretical models describing nuclei are far from being complete, and nuclear structure physics experiments are essential to further improve our theoretical understanding of the behaviour of nuclear matter.

This thesis work encompasses the experimental study of the short-lived neutron-deficient radioactive nickel isotope  $^{54}\text{Ni}$ . The experiment in focus was conducted during march 2006 as a part of the "Rare Isotope Investigation" (RISING) campaign at GSI. On the following pages I will outline the physical background of the experiment, describe the experimental techniques in Chapter 3, and depict the experimental setup used in this study in Chapter 4. The main focus of this work is Chapter 5, in which I delineate the process of preparing an experiment such as the one performed, by means of simulations. Chapter 5 is an initiative to write a users guide for the simulation program MOCADI, while Chapter 6 concentrates on the actual results of the simulations carried out. In Chapters 7 and 8, I will provide a brief overview of the preliminary analysis of the experiment, as well as shortly comment on the results of the experimental data from the experiment.



## Chapter 2

# Physical Background

In nuclear structure physics, mainly two forces of nature are considered: the strong force, and the electromagnetic force. While the strong force works as an attractive force between nucleons (protons and neutrons), the electromagnetic force counteracts this as the positively charged protons experience a Coulomb repulsion. When the Coulomb repulsion in a nucleus becomes dominant, the nucleus is dismembered. A more subtle force to reckon with is the weak force, which is responsible for the  $\beta$ -decay of instable nuclei. A nucleus spontaneously  $\gamma$ -decays, i.e. emits a high-energy photon, if its total energy is higher than its ground state energy. These emissions are discrete transitions that reveal the structure of nuclei. To study the to first order charge independent strong force interaction between nucleons in a nucleus, it is appropriate to look at differences of systems with mirror symmetry [1] [2]. For this, the structure of the systems has to be known through their level schemes. Some more details of the physical background of the experiment this work focuses on will briefly be summarised below.

### 2.1 Mirror Nuclei

By neglecting the Coulomb interactions inside the nucleus, protons and neutrons are thought to behave in the same way regarding strong force interactions. Protons and neutrons can thus be seen as two states of the same particle: the nucleon with isospin  $t = 1/2$ . The proton can be assigned the isospin projection quantum number  $t_z = -1/2$  and the neutron  $t_z = +1/2$ . The repulsive Coulomb force, however, breaks the isospin symmetry since the proton no longer is the mirror image of the neutron. This breaking of isospin symmetry can be studied in mirror nuclei. Mirror nuclei are pairs of nuclei that have mirrored proton/neutron numbers; for example, the pair  ${}^{54}_{28}\text{Ni}_{26}$  and  ${}^{54}_{26}\text{Fe}_{28}$ . These pairs of nuclei should have very similar energy level schemes, and it is the difference between them, that can be used for deducing properties and behaviour of nuclear matter in general.

## 2.2 Isomeric States

The lifetimes of excited states in a nucleus are usually of the order of femto- to picoseconds ( $10^{-15}\text{s}$ – $10^{-12}\text{s}$ ), but just like in atomic physics, there exist metastable states that have considerably longer lifetimes than normal excited states. These are so-called isomeric states [3], which live for several nanoseconds up to the order of seconds and even years in rare cases. The decay probability of an excited state depends on many factors like energy difference, where a larger energy difference gives a higher decay probability, or large changes in spin or nuclear deformation, which can lead to a hindrance of the  $\gamma$  decay. Isomeric states have to be populated either directly or fed by decays of levels at higher excitation energies of the nucleus. It is the isomeric states that make possible the experimental technique (cf. Chapter 3) applied in the stopped beam RISING campaign, where excited states are produced via projectile fragmentation (cf. section 3.2).

## 2.3 Branching Ratios

A branching ratio is the ratio between the decay probability of one individual decay branch and the total decay probability. Partial decay constants,  $\lambda_i$ , are defined as the branching ratio times the total decay constant. The sum of all partial decay constants then equals the total decay constant for the decay including all its branches,  $\lambda = \sum \lambda_i$ . Branching ratios become evident if there are two detectable competing decay channels which have half-lives that are of the same order of magnitude. As we will see, in the case of  $^{54}\text{Ni}$ , there are several competing decay channels from an isomeric  $I^\pi = 10^+$  state.



## Chapter 3

# The RISING Stopped Beam Campaign

The  $^{54}\text{Ni}$  experiment, which is the focus of this work, is part of the stopped beam campaign within the Rare Isotopes Investigations (RISING) at GSI. Three stopped beam experiments were performed at GSI during February and March 2006. In this chapter I will provide a short overview of the general experimental techniques applied. In section 3.3 more specific issues related to the  $^{54}\text{Ni}$ -experiment are addressed.

### 3.1 Intent

The stopped beam campaign uses isomer spectroscopy for studies of the internal structure of short-lived radioactive nuclei produced by means of relativistic projectile fragmentation at beam energies of  $\sim 500$  to  $1000$  MeV/u. The projectile beam provided by the SIS synchrotron at GSI, is impinged on a target to produce exotic nuclei in excited states. The produced ions are separated and identified in-flight in the magnetic forward spectrometer FRS, which is described in some detail in Chapter 4. The resultant radioactive secondary beam is stopped in layers of matter at the final focal plane of the FRS, where 15 clusters of high efficiency germanium detectors map the decay of the implanted ions in the stopper.

### 3.2 Experimental Method: Fragmentation

Projectile fragmentation occurs when a projectile nucleus, accelerated to energies far above the Coulomb barrier potential, collides and strongly interacts with a target nucleus. At the high beam energies used in the RISING experiments, the fragmentation process can be described as a two-step reaction, the so-called abrasion-ablation process [4]. In the abrasion step, which occurs on a nuclear timescale within approximately  $10^{-21}$  s, the overlapping regions of the nuclei, the "participants" in the reaction, are cut off.

The remnant of the fragment, called "spectator", remains more or less untouched and undergoes an ablation phase which lasts some  $10^{-16}$  s. In this step, the nucleus evaporates particles and  $\gamma$ -decays until reaching the ground state or, until being trapped in an isomeric state.

Due to the violent reaction mechanism and the large amounts of energy involved in this process and different impact parameters, a wide variety of fragments can be produced; essentially everything from pick-up reactions to completely disrupted nuclei. Typically the kinetic energy per nucleon of the fragments is very close to the pre-reaction energy per nucleon of the projectile. The most favourable reaction products of fragmentation reactions follow the line of beta-stability, and hence, if a stable beam is fragmented, the production cross section for drip-line nuclei is low.

### 3.3 $^{54}\text{Ni}$ Experiment

The goal of the  $^{54}\text{Ni}$  experiment is to map the energy level scheme of  $^{54}\text{Ni}$  up to its, by mirror symmetry predicted, isomeric  $10^+$  state. The branching ratio between the expected electric quadrupole ( $E2$ ) and electric hexadecapole ( $E4$ )  $\gamma$  decays of the  $10^+$  state, and its lifetime should also be determined. For the experiment to be possible, the fragmentation of the projectile must produce reasonable quantities of  $^{54}\text{Ni}$  in excited states with a nuclear spin of  $I \leq 10$ . As a rule of thumb, the more nucleons that are removed from the projectile, the higher the spin that can be produced. At the same time the production cross section decreases the further away the projectile is from the fragment of interest.

A natural choice of beam would be the at GSI frequently used  $^{58}\text{Ni}$ , which would imply a removal of four neutrons to produce  $^{54}\text{Ni}$ . B. Blank *et al.* [5] conducted an experiment in 1994, experimentally measuring cross sections of proton-rich nuclei ranging from Ni to Sc for isotopes from near the line of stability out to the proton drip-line. The authors show that the measured production cross section of  $^{54}\text{Ni}$  is  $1.2 \cdot 10^{-2}$  mb, as compared with the result obtained with the empirical code EPAX 2.1 [6], which underestimates the production cross section slightly with a predicted value of  $7.7 \cdot 10^{-3}$  mb. With the available  $^{58}\text{Ni}$  beam intensity at GSI, which is of the order of  $5 \cdot 10^8$  particles per second, the measured cross section would imply a production rate of 1600  $^{54}\text{Ni}$  ions per second using a 4 g/cm<sup>2</sup> Be target, or 400  $^{54}\text{Ni}$  ions per second, using a 1 g/cm<sup>2</sup> Be target. Both cases make possible the gathering of large statistics, while simulations, discussed in Chapter 5, show that the 1 g/cm<sup>2</sup> Be target is the best choice for the experiment.

By choosing the  $^{58}\text{Ni}$  beam, there is one crucial issue that needs to be clarified. Is the removal of only a few nucleons able to populate the  $10^+$  isomer in  $^{54}\text{Ni}$ ? To get feedback on this topic, we contacted Prof. Marek Pfützner, and refer to [7] and an e-mail of his.

*” Indeed, our simple model for isomeric ratios would say that the more distant beam from the fragment, the higher the population of the isomer. But this is not a strict rule. One example is very promising for your case: with Schmidt-Ott (Z.Phys. A 350 (1994) 215) we have produced a  $19/2^-$  isomer in  $^{43}\text{Sc}$  by fragmentation of  $^{46}\text{Ti}$ . The population was quite large, changing from about 1% in the center of the momentum distribution to 12% at the wing of the distribution. [...] With the  $^{58}\text{Ni}$  beam it should be easy to collect large statistics and the identification of the  $^{54}\text{Ni}$  should be much easier than with heavier beams. [...] Actually, such a try to populate a  $10^+$  state by  $4n$  removal only, would be a very interesting test in itself! “*

— Marek Pfützner

Further discussion of experimental parameters and optimisation of an experimental setting is found in section 6.3.



## Chapter 4

# Experimental Setup

The experimental setup utilised in the RISING Stopped Beam Campaign, outlined in Chapter 3, is placed within the Gesellschaft für Schwerionenforschung (facility for heavy-ion research), GSI, located in the vicinity of Darmstadt, Germany. In this setup the SIS synchrotron can accelerate ions provided by an ion source to a maximum magnetic rigidity of  $B\rho = 18 \text{ Tm}$ , which corresponds to an energy of  $1.0 - 4.5 \text{ GeV/u}$  depending on which ion species is accelerated. The beam is then extracted from the synchrotron and can be supplied to various experimental areas. The *FR*ragment Separator FRS [8] is the central tool used for in-flight separation and analysis of nuclear reaction products.

### 4.1 The FRS

The FRS is a 71 m long achromatic magnetic forward spectrometer that consists of four independent sections of ion optics, comprising bending and focusing magnets. In the following I will provide a brief overview of the design and function of the FRS. A schematical drawing of the FRS is shown in Fig. 4.1.

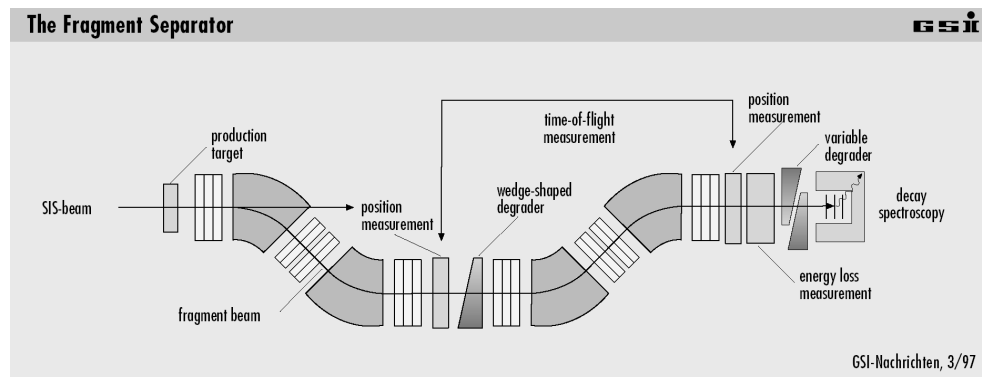


Figure 4.1: An overview of the fragment separator FRS at the GSI facility.

### 4.1.1 Function and Concept

The design of the FRS relies on the concept of magnetic rigidity. Magnetic rigidity  $B\rho$ , is a measure of magnetic bending resilience and depends on ionic charge, mass and translational energy - less charge, higher mass and higher kinetic energy yields a higher magnetic rigidity and vice versa. As a certain reaction product can be produced in different ways and at varying depths in the production target, any given produced ion species has a spatial, angular, and momentum distribution when it leaves the production target in front of the FRS. (The maximum momentum acceptance of the FRS allows for an optical transmission efficiency in excess of 90%)

The first two sections of the FRS separate the reaction products as a function of their magnetic rigidity, utilising sets of focusing and bending magnets. This yields a mass over charge,  $A/Q$ , separation. At energies of 0.5–1.0 GeV/u, light and intermediate mass ions, ( $A \leq 100$ ) usually have only one charge state:  $Q = Z$ , i.e., all their electrons are fully stripped off. For heavier ions there may be several charge states in one experimental setting, each charge state having a different  $A/Q$  value, and thus position. Typically these are hydrogen-like (one electron) or helium-like (two electrons) charge states.

In the middle of the spectrometer, the second focal plane, an energy degrader is used to separate the incoming ions as a function of the square of their charge,  $Q^2$ , according to the Bethe-Bloch formalism [9], seen in equation 4.1, which approximates the energy loss per distance traveled:

$$-\frac{dE}{dx} = \frac{4\pi}{m_e c^2} \cdot \frac{nZ^2}{\beta^2} \left( \frac{e^2}{4\pi\epsilon_0} \right)^2 \cdot \left[ \ln \left( \frac{2m_e c^2 \beta^2}{I \cdot (1 - \beta^2)} \right) - \beta^2 \right], \quad (4.1)$$

where  $n$  is the electron density of the target,  $\beta = v/c$ , and  $I$  is the mean excitation potential of the target.

Yet, directly after the degrader, this separation is not spatial. In order to have a spatial separation, the ions passing through the degrader again are separated as a function of their magnetic rigidities in the second half of the FRS.

At the final focal plane of the FRS, all ion distributions then have different spatial positions and can be resolved. To have well separated, narrow distributions, the FRS can be run in an achromatic mode [8]. For this mode, the correct setting of the wedge-shaped energy degrader angle is significant, which will be described in more detail below. An alternative optical mode is the so-called monochromatic mode. Ion distributions in this mode have poor spatial resolution but a very narrow momentum distribution at the final focal plane.

### 4.1.2 Ion-Optics

Each of the four sections of the FRS consists of one 30° dipole bending magnet, an arrangement of five quadrupole magnets for first order focusing, and two sextu-

pole magnets, one in front and one behind the dipole, for second order aberration corrections. Each section has a focal plane that can be used for slits, detectors, and degraders. At the second focal plane the dispersion reaches its maximum with  $\sim 7$  cm per percent of momentum deviation. The third and fourth ion-optical sections again yield a separation as a function of magnetic rigidity, after which the residual ion distributions in the secondary beam are focused at the final focal plane.

### 4.1.3 Component Overview

Moving downstream along the beamline of the FRS, the following elements are found.

- **Target Area:** Penetrating the SIS vacuum window leading to the FRS, the primary beam enters the target area. The beam then hits one of the different production targets [10], mounted on a target ladder, that remotely can be moved into the beamline.
- **S1 Area:** Passing through the first ion optical section, the beam reaches the first focal plane. Here, the frequently used S1 slit is located.
- **S2 Area:** At the second focal plane resides the so-called Sc21 scintillator, the S2 slit, and a wedge shaped energy degrader. Additional components like stripper foils or detectors optionally can be mounted on a ladder located behind the wedge.
- **S3 Area:** The third focal plane resembles the S1 area. Usually it is not used for more than its S3 slit.
- **S4 Area:** At the end of the FRS, the final focal plane is used for an experiment's detector setup and for particle identification with detectors described in section 4.2. The S4 components are sitting in air, which does not make much of a difference at the relativistic ion energies, but yet the amount of air has to be considered for proper implantation of the ions in a stopper.

All FRS components like slits, ladders and degraders are remotely tunable and all components in the beamline can be removed in that manner.

### 4.1.4 A special component: the Wedge Degrader

Figure 4.2 displays the wedge-shaped energy degrader. This is an essential part of the FRS setup. The device comprises three different degrader parts, all precisely machined from aluminium and remotely tunable [11] independently from each other:

1. **Disk** The disk device is a set of two different, thin, inclined disks that can be rotated against each other to create a range of angles.
2. **Wedge** The second device consists of two wedges that can be shifted vertically in order to generate different thicknesses. The resulting minimum thickness is 1 mm and the maximum thickness is 25 mm.
3. **Ladder** Five different constant-thickness plates are mounted on a ladder, which is used when an exceptionally thick degrader is required. The thicknesses are 16 mm to 80 mm of aluminium, in steps of 16 mm in between those values.

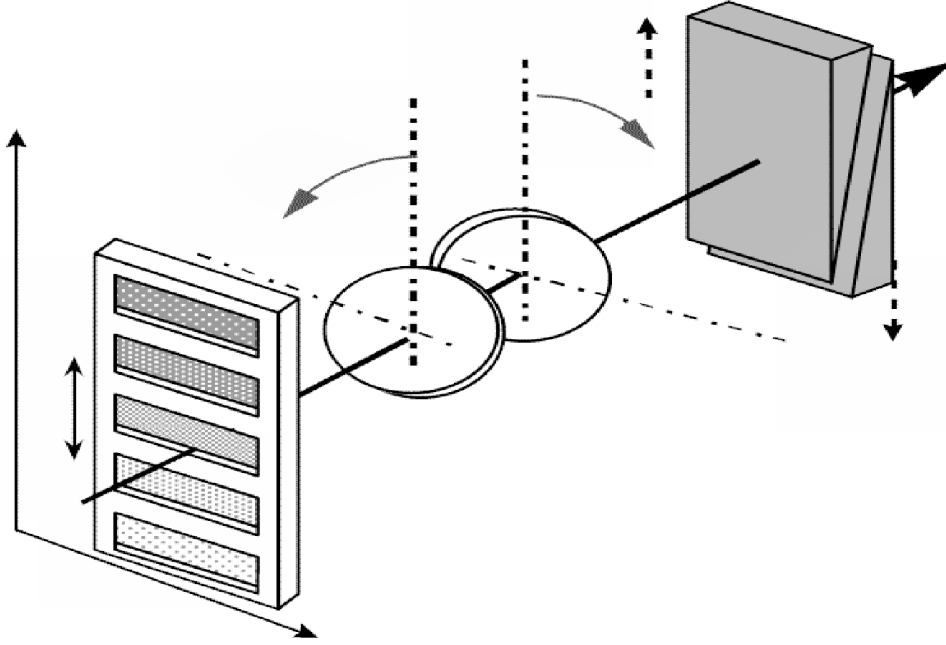


Figure 4.2: Three degrader devices at S2. Together they yield a fully tunable wedge degrader. Illustration from [12].

## 4.2 Particle Identification

A crucial part of every experiment at the FRS is the correct in-flight identification of the nuclear reaction products. For this to be achieved, a variety of detectors is used, most of them mounted on a special table in the S4 area, after the final ion optical section of the FRS, and prior to its final focal plane. The measurables that are used for correct identification are the ion positions at the second and final focal plane, the time of flight between the Sc21 scintillator at the second focal plane and the Sc41 scintillator at the final focal plane, and the energy loss of the ions in an ionisation chamber in the S4 area, outlined in Fig. 4.3.

### 4.2.1 Scintillation Detectors

For the purpose of time-of-flight and position measurements, fast plastic scintillation detectors are installed at the second and final focal plane of the FRS. Scintillator 21 at the second focal plane installed for our experiment is a 3.39 mm plastic scintillator. It is read out from four sides to give both the  $x$ - and  $y$ -position of a passing ion. Sc41 is read out in the same way as Sc21, while Sc42 is read out from left and right only, and the final, veto Sc43 from one side only.



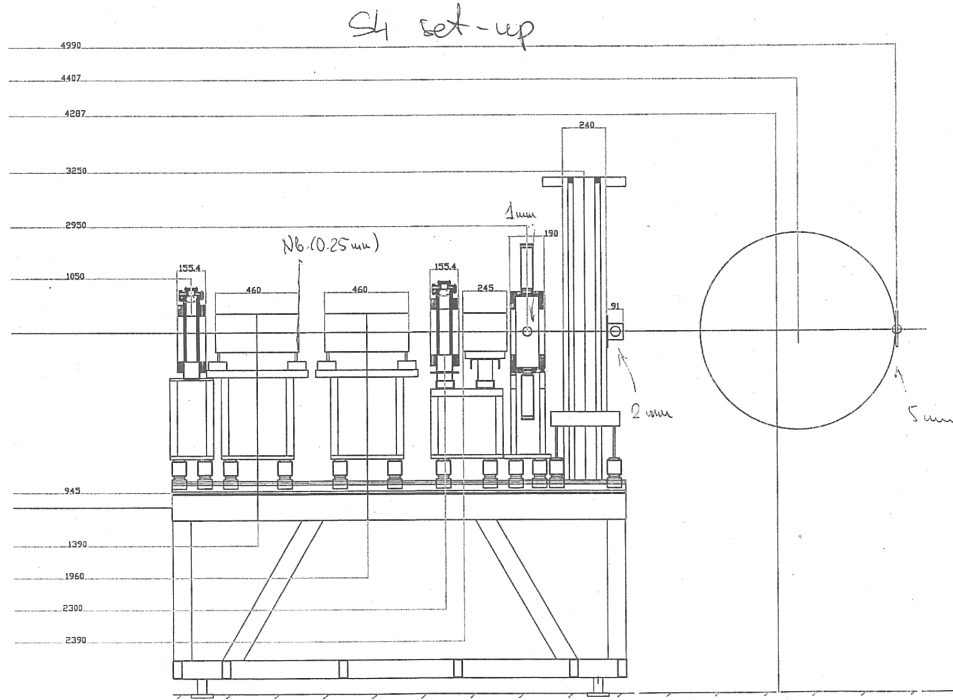


Figure 4.3: Technical drawing of the S4 table and the detectors used at S4. All distances are measured from the exit of the final quadrupole magnet. Moving from the final quadrupole magnet downstream, i.e. toward increasing distances in the drawing, the different components are: MW41, MUSIC41, MUSIC42, MW42, S4 Slit, Sc41, Degrader, Sc42, Stopper, Sc43. The use of the detectors is described in the text.

For the time-of-flight measurement, the 1 mm thick Sc41 gives the start signal and the delayed signal from Sc21 marks the stop of the measurement. This counter intuitive way of measuring the time of flight ensures that the data stream is not swamped with events. The general rule for time-difference measurements is to start the clock with the detector counting least. A 2 mm thick scintillator, Sc42, is placed behind the degrader to measure if the ions survived the slowing-down process. The final scintillator in the setup, the 5 mm thick Sc43, is installed behind the stopper to detect ions that were not implanted in the stopper.

### 4.2.2 Multiwires

The Multiwire, MW, detectors in the FRS setup are used for the measurement of the  $x$ - and  $y$ -positions of passing ions. The detector [13] consists mainly of a gas chamber filled with a CO<sub>2</sub>/Argon mixture and three thin wire grids. The electrons from ionisations in the detector gas, which are caused by passing ions, are collected by an anode grid. In this way the position of the passing ion can be determined. The typical position resolution of the MW detectors is about 0.5 mm and the detectors cover an area of 20 × 20 cm.

MW detectors are mounted in pockets at S1, S2, and S3. These detectors have 100 μm thick titanium vacuum windows to screen the FRS vacuum. Two MW can be mounted on the S4 table, MW41 and MW42. Situated in air, 25 μm thick kapton windows are used instead of titanium windows.

### 4.2.3 MUSIC

The *MU*ltiple *S*ampling *I*onisation *C*hamber outputs the amount of ionisation caused by a passing ion. The detector gas is composed of 90% of argon and 10% methane. The ions and electrons produced in the ionisations drift toward the cathode and segmented anode respectively. The produced charge is proportional to the square of the passing ions' charges, and thus gives a measure of nuclear charge if the ion is fully stripped. For this reason, two MUSICs are set up at S4 in this experimental campaign. Ions are likely to change their charge state when not fully stripped, while passing through the layers of matter between the MUSICs. This helps the correct identification of heavy ions' nuclear charge  $Q$ .

## 4.3 Stopper and Implantation

At the final focal plane of the FRS, the beam can be stopped with a so-called catcher or stopper. In the case of the <sup>54</sup>Ni experiment, a 4 mm thick beryllium plate was used for this purpose. In this experiment, the goal is to implant all incoming <sup>54</sup>Ni ions in this plate. Ions with too low energy will be stopped in layers of matter prior to the stopper, while ions with too high energy will pass right through it. Ions passing through the stopper are detected by Sc43, which is used as a veto detector. Making use of MOCADI and LISE++ simulations (cf. Chapter 5) and the veto detector, one can ensure that the ions are properly implanted. The stopper is located at the center of the array of germanium detectors.

## 4.4 Ge-Detectors

An array of 15 EUROBALL [14] cluster detectors in closed formation is mounted around the final focal plane of the FRS. Each of the clusters has seven individual germanium crystals, adding up to a total of 105 crystals. Each crystal has its own set of electronics and the array has an overall 1 MeV peak efficiency in excess of 15%. A photograph of the opened array can be seen in Fig. 4.4.

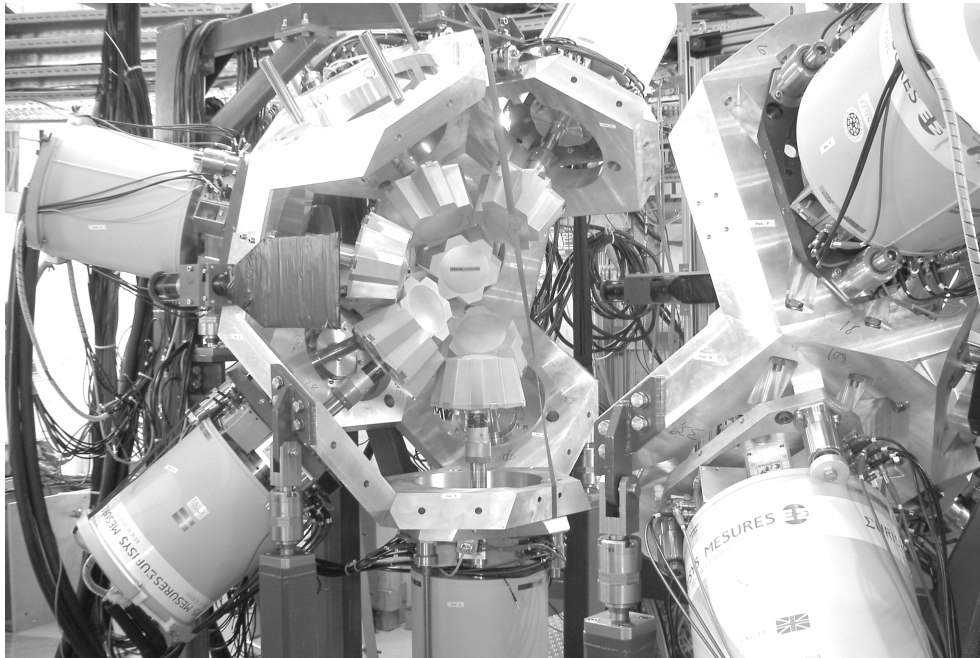


Figure 4.4: The opened Ge-detector array still missing one EUROBALL cluster at the upper left. Note the swedish cluster in the lower left of the picture.



# Chapter 5

## Simulations

Nuclear structure physics experiments using the FRS are always preceded by simulations of the experimental setup. For this purpose, MOCADI [15] was developed in the late 1980's. With this Monte Carlo code, the complete path of heavy ions can be tracked throughout the simulated setup. This includes ion distributions, transmission rates, energy loss in materials, and other important parameters like time of flight and implantation depth.

A more recent effort is the program LISE++ [16], which provides the user with a complete and intuitive graphical interface to build and run simulations. With its ability to run a Monte Carlo code, simulating a setup with certain settings, and simultaneously plot the results, it is a valuable tool for rapid analysis, especially during an experiment.

Although MOCADI cannot be considered to be as intuitive and user friendly as LISE++, it is more precise in the simulation of the ion optics, and hence, despite the program's age, still used for the preparation of secondary beam experiments. Today both programs are used by the experimental groups: MOCADI is used for rigorously simulating and tuning an experimental setting well ahead of the experiment. LISE++ on the other hand is used during the process of FRS calibrations and to see quickly what a certain change in the setting would imply in terms of the position and yield of isotope distributions. Neither MOCADI nor LISE++ require the user to have programming skills.

This chapter has the aim to give a thorough introduction to MOCADI. The focus of section 5.1 will be on how to build a simulation of an experimental setup, for the purpose of creating a suitable setting for an experiment utilising the FRS, which was described in Chapter 4. Section 5.3 will describe a simulation's output file and section 5.4 focuses on how to create a setting with the information obtained from an output file. In order to give the reader a complete overview, I will also briefly cover the basics of LISE++.

## 5.1 MOCADI

MOCADI relies on a simple concept of operation. The user writes an input file as a plain text document with the file extension `.in` and directly sends it to the MOCADI executable via the command `mocadi filename.in`. After this command, MOCADI is completely self-going and produces output files in accordance to the keywords used in the input file. When the simulation finishes successfully, the user can analyse the results by examining the standard output file of the simulation. This has the format `filename.out` and is a plain text document as well.

While MOCADI proves to be easy to use once the basics are understood, its operation is not self-evident, and thoroughly commented input files seem to be almost non-existent. For this reason I provide solid, well commented examples of MOCADI's building blocks of an input file. The examples I supply come from an input file I created for the  $^{58}\text{Ni}$  fragmentation experiment described in the previous chapters. The complete, commented input file can be downloaded from my homepage [17]. As an additional and complete source of information I refer to the online MOCADI manual [15].

## 5.2 Implementation

Before starting to write input files, one should be aware of their general structure and what coordinates MOCADI uses for parameterisation.

A `.in` file is constructed by the use of keywords and so-called cards. The keywords are used for the initialisation of important functions of MOCADI. For example the keyword `EPAX 2` will ensure that MOCADI uses the cross sections given by EPAX 2 calculations. Cards on the other hand are used as building blocks of the experimental setup to be simulated. An example is the `MATTER` card, which specifies a region of matter in the path of the beam particles. In the given examples, I will frequently make use of the asterisk symbol, `*`, which in MOCADI is used to comment in the code. Anything after this symbol will be ignored in that particular line. For commenting out more than one line, `/* ... */` is used instead.

In MOCADI the  $z$ -axis is the beam axis, which always runs along the center of the beamline. The  $z$ -value is zero at the point where the `BEAM` card starts the simulation. The  $z$ -value increases downstream. The  $x$ -axis parameterises the dispersive axis of the FRS and is always perpendicular to the  $z$ -axis. When looking downstream, the left-hand side is positive in  $x$ , while the right-hand side is negative in  $x$ . Both LISE++ and MOCADI use this convention. The parameterisation of the *real* FRS is the opposite in  $x$  though, which can lead to confusion, especially when setting slits. The  $y$ -axis is positive pointing upwards and negative pointing down.

### 5.2.1 Initialisation

The normal start to a simulation input file is the initialisation of important parameters by the use of the proper keywords. Figure 5.1 shows a standard initialisation of the simulations I created for the RISING Stopped Beam Campaign. Simulations have to be initialised by keywords that specify output formats, programs for the calculation of energy loss and production cross sections, and the location of the matrix files describing the ion optics.

```
***** Initialise Simulation *****
option listmode rwn
                                * How the .hbk output file is arranged.

atima-1.0                       * For calculating energy loss in material.
EPAX 2                           * For calculating reaction cross sections.

MATRIXFILE                       * This card initializes the ion optics.
/usr/local/mocadi/matrix/        * Path of the .MAT files for the ion optics.

*****
```

Figure 5.1: *These keywords define which resources MOCADI should use.*

In the initialisation shown in Fig. 5.1, the first keyword determines the output format of a HBOOK histogram file used when saving the status at a certain position of the simulated setup with the keyword `SAVE`. Saving is addressed in section 5.2.6. The `atima-1.0` keyword marks that the program `ATIMA` is used for calculating the energy loss of ions in matter of all kind, including frequently used compound materials like plastics and special gases like Carbon Tetrafluoride in detectors like the `MUSIC`. `EPAX 2` is a program needed for the calculation of reactions cross sections. The last keyword `MATRIXFILE` specifies the location of the matrix files describing the ion optics. Appropriate matrix files can be downloaded from the GSI website [15].

### 5.2.2 The Beam, Target and Fragment Card

In order to implement an experimental setup correctly, it is important to be aware of the units MOCADI uses. Table 5.1 summaries, which units are used for different quantities. In some cases, for example the MATTER card, the user can choose which units should be used:

Table 5.1: *Units used in MOCADI*

| Quantity  | Unit                  | Quantity | Unit                  | Quantity          | Unit   |
|-----------|-----------------------|----------|-----------------------|-------------------|--------|
| Energy    | [MeV/u]               | Mass     | [u]                   | Energy Loss       | [MeV]  |
| Distance  | [cm]                  | Time     | [ $\mu$ s]            | Angle             | [mrad] |
| Thickness | [mg/cm <sup>2</sup> ] | Density  | [mg/cm <sup>3</sup> ] | Magnetic Rigidity | [Tm]   |

The actual start of the simulation is marked by the BEAM card. This card is used to create a beam of one particular isotope, in this case <sup>58</sup>Ni. The beam is created as exemplified in Fig. 5.2. The BEAM card incorporates a wide variety of parameters: from the basic parameters that set the isotope and the beam energy, to spatial distributions, angular distributions and the particle distribution in energy and time.  $t_0$  is the starting time of each simulated particle.  $X$  and  $Y$  are particle positions and  $A$  and  $B$  movement angles measured from the beam axis  $z$ . The parameters used in this case simulate a reasonable beam quality.

```
***** Beam Specification *****
BEAM                               * Starts the beam specification
10000                              * Number of particles to be simulated
550.0, 0., 58.0, 28, 0             * Energy, t_0, A, Z, number of electrons
4,                                 * Beam distribution in X (4 = uniform ellipse)
0.2, 10.0, 0.0, 0.0, 0.0         * max width, max angle, r_{XA}, X_0, A_0
4,                                 * Beam distribution in Y (4 = uniform ellipse)
0.2, 10.0, 0.0, 0.0, 0.0         * max width, max angle, r_{YB}, Y_0, B_0
1                                  * Beam distribution in E&t, 1 = uniform
0.0, 0.0, 0.0, 0.0, 0.0         * width E, width t, r_{ET}, E_1, t_1

* The units used are: MeV/u, microseconds, centimeter, milliradians
*****
```

Figure 5.2: *The BEAM card marks the start of the simulation.*

After the beam is specified, the production target is implemented with the TARGET card, which is illustrated Figure 5.3. The fragmentation process is not simulated with the actual cross sections, because of the huge number of beam particles that would be required. Instead the program 'splits' the beam. This works as follows. Say the particle number specified with the BEAM card is  $N$ . If our FRAGMENT card (see Fig. 5.4), which tells MOCADI which isotopes we want to simulate, contains six entries, then  $N$  particles of *each* of the listed isotopes are produced in the production target. In addition to in this case  $6 \cdot N$  particles, the  $N$  primary beam particles will be simulated by MOCADI, as well as  $N$  setting fragment particles, that will be produced even though not listed in the fragment list.



As the TARGET card in Fig. 5.3 indicates, the present setting fragment is  $^{54}\text{Ni}$ . The setting fragment is the fragment for which the ion optics are optimised. If the user prefers to skip the simulation of primary beam particles that have not reacted in the target, the PRIMARY\_BEAM card should not be used (see Figure 5.4).

```
***** Target Specification *****
TARGET                                * Starts the target specification
9, 4, 1850,                            * A, Z, Density [mg/cm3]
54, 28,                                * Fragment Mass [u], Fragment Z
5, 4007                                * Mode=5: Thickness in [mg/cm2], Thickness
1, 1, 1, 1, 1, 0                      * Toggle: Scattering, Stragglng, Momentum
                                        *      Distribution, Coulomb Scattering,
                                        *      Energy loss, Fission
*****
```

Figure 5.3: The TARGET Card determines the characteristics of the production target and the physical models used for the simulation of the fragments. In fission simulations, make sure the last parameter in the last line of the TARGET card is set to 1.

```
***** Fragments and Primary Beam Particles *****
FRAGMENT                               * Calculation of all fragments listed
2, 6                                    * Mode=2: List Mode, Number of entries
28, 55                                  * Fragment: Z, A
28, 53
27, 53
27, 52
26, 51
26, 50

PRIMARY_BEAM                            * Comment out ("0") to stop simulating
0                                        * primary beam particles after the target.
                                        * 0: Atomic charge states are calculated
                                        * in the same way as for the fragments.
*****
```

Figure 5.4: The FRAGMENT card determines which fragments MOCADI simulates. The PRIMARY\_BEAM card enables the simulation of unreacted projectile particles.

### 5.2.3 Implementation of Ion Optics and Slits

The program GICO can be used for the calculation of the ion optical transfer matrices [15], which are implemented as shown in Figure 5.5. The FRS makes use of three different types of magnets: dipole magnets that serve as dispersive elements in the optics and give rise to the  $A/Q$  separation of the FRS, quadrupole magnets for focusing, and sextupole magnets for higher order corrections.

Because of the physical extent of the beampipe, collimators must be used to restrict the flight paths of the ions. In Fig. 5.5 this is done with collimators, the `COLL` card, that exactly resemble the extent of the beampipe. In the MOCADI implementation of the ion optics, the magnetic fields are often divided into magnetic fringe and main field matrices to render better accuracy. The available parameters govern the characteristics of the setting fragment, and have to be inserted by the user. The ion mass, charge and energy at this particular spot have to be supplied in order for the simulation to work properly.

A sextupole magnet is implemented in exactly the same way as a quadrupole magnet shown in Fig. 5.5. A dipole magnet at the FRS is implemented with the following components: a rectangular position collimator (Collimator Shape = 1) followed by a magnetic fringe, the main field, and another rectangular position collimator at the center position. Adding the inverse order of these elements: main field number two, magnetic fringe and a collimator, completes the dipole implementation. Examples of all three implemented ion optical building blocks are available in the full sample file [17].

When the whole setup is built, it can easily be tuned by changing the calibration energy of the magnets. The setting fragment will always stay centered as long as the setting is correct - including appropriate matrices - and the magnets are tuned for that specific fragment's energies throughout the FRS. Changing the calibration energy is done through changing the third parameter in the second line of all `MATRIX` cards in an optical section of the setup. This changes magnetic field strengths and hence, the fragment positions shift due to the change in the dipole fields. This is frequently used in both MOCADI simulations and in practice.

In practice this shifting is done by scaling the magnetic rigidities of the FRS magnets, the  $B\rho$  values. This has the effect of bending the trajectory of the fragments more or less. Setting the energy to a higher value will increase the dipole magnets'  $B\rho$  values and thus their bending power. At a certain energy, a specific ionic isotope has a unique  $B\rho$  value, which, after the simulation is completed, can be found in the MOCADI output files. The  $B\rho$  values are the most important parameters in the process of creating a FRS setting for an experiment.

Another vital element in the process of creating a simulation are slits, created with the `SLIT` card. Just as collimators, this card blocks the path of ions which are outside of a specific range in position space at a certain  $z$ -value. The implementation of these elements is simple: inserting the minimum coordinate value, maximum coordinate value for first  $x$ -position and then  $y$ -position, cuts all particles outside of that range. This is shown in Fig. 5.6.

Of course, all these elements cannot be packed on each other ignoring the physical distance between them. The drift-lengths have to be correct in order for the optics to work properly. The `DRIFT` card, presented in Fig. 5.7, marks a distance that particles have to travel through perfect vacuum before they reach the next event, i.e. the next card. In the case of the FRS, the drift lengths have been measured to very high accuracy and should be taken from the standard input files found at the MOCADI

```

***** FRS Special Position Collimator *****
COLL
4, 0, 0, 12.4, 12.58, 7.47      * Collimator Shape, X_0, Y_0, X_{max},
                                * Y_{max}, sig_fac (only used for Shape 4)

***** Magnet TS2QT11 *****

MATRIX                          * Initialising an optical transfer matrix
R811001.MAT                      * Matrix filename
53.95791, 28, 520.3250           * Reference particle: A, Z, E [MeV/u]
3, 3                             * 'th order used in calculation. 3 is max.

MATRIX                          * Magnetic Fringe: 001.MAT
R811002.MAT                      * Main Field:      002.MAT
53.95791, 28, 520.3250           * Magnetic Fringe: 003.MAT
3, 3

MATRIX
R811003.MAT
53.95791, 28, 520.3250
3, 3

***** FRS Special Position Collimator *****

COLL
4, 0, 0, 12.4, 12.58, 7.47      * Collimator Shape, X_0, Y_0, X_{max},
                                * Y_{max}, sig_fac (only used for Shape 4)

*****

```

Figure 5.5: *The implementation of the matrices resembling a quadrupole magnetic lens. This, including the collimators, can be seen as one ion optical 'building block'.*

homepage [15].

If the ions pass a region where there is no vacuum or low vacuum, these conditions can be simulated by the use of the DRIFT-IN-GAS card, as seen in Fig. 5.8. This card should also be used for the simulation of detector gases. For special gases, one chooses the so-called List Mode by setting the second parameter to zero and the third one in accordance to the list of materials and gases found in the MOCADI manual [15]. If it is a simple, one-element gas, then the second and third parameter represent the atomic mass and the atomic number, respectively.

```

***** Slit *****

SLIT
-100.0, 100.0, -100.0, 100.0    * X min, X max, Y min, Y max

*****

```

Figure 5.6: *The SLIT card makes a cut in position space. These values correspond to wide open slits in both  $x$ - and  $y$ -position.*

```

***** Drift in Vacuum *****
DRIFT                               * Distance [cm] the beam has to travel in
225.1175260                         * vacuum before reaching the next event.
*****

```

Figure 5.7: *The DRIFT Card.*

```

***** Drift in Gas *****
DRIFT-IN-GAS
14.20, 0, 202, 17.097               * Length [cm], Mode: List, Air, [mg/cm2]
1, 1                                * Toggle on/off: Scattering, E-Stragglng.
*****

```

Figure 5.8: *This card creates a gas with a certain extent in the  $z$ -coordinate.*

### 5.2.4 Matter, Wedge Degradar and Implantation

An important aspect of every experiment at the FRS is the matter in the path of the secondary beam. For the simulation of intervening sections of matter, the **MATTER** card is used. Two examples showing how to use this card are provided in Fig. 5.9. The most important parameters determine the element - or compound - and its thickness, i.e. its extent on the  $z$ -axis. Two different thickness modes let the user choose from either supplying the thickness in  $[\text{mg}/\text{cm}^2]$  or in  $[\text{cm}]$ . In both cases the density of the matter, measured in  $[\text{mg}/\text{cm}^3]$ , has to be entered. Implementing detectors, the different layers of matter can easily be stacked by creating multiple **MATTER** cards, each card corresponding to one layer of material.

At the second focal plane of the FRS, the wedge-shaped energy degrader is located. In MOCADI, the setting of this vital part of the FRS is made easy by the **WEDGE** card, which is shown in Fig. 5.10. Its setup differs only slightly from that of the **MATTER** card; the main difference is one line that defines the thickness dependence on the  $x$ -coordinate. The first line defines the material and the second line the thickness as follows. The center thickness, in the units chosen in line three, is defined by the first parameter. The second parameter gives the linear dependence on the  $x$ -coordinate as described in the comment in Fig. 5.10. Using a non-zero third parameter in this line, would give the wedge thickness a quadratic  $x$ -dependence as well. This cannot be used in practice in FRS experiments, and hence renders this parameter useless for our purpose. Usually the linear dependence on the  $x$ -coordinate is referred to as an angle, which is positive in the case of the FRS and normally a few milliradians in size.

```

***** SCI21 Plastic Scintillator *****
MATTER
0, 201, 1032          * A=0: List Mode, Plastics, Density [mg/cm3]
2, 0.339             * Mode=2: Thickness in [cm], Thickness
0, 0, 0             * Geometry Mode 0: Homogeneous
0, 0, 0             * Shift in: x-direction, y-direction, angle
1, 1                * Toggle on/off: Scattering, E-stragglng
0, 0, 0, 0          * Matter thickness random mode: 0 = off

***** Aluminium Degradr *****
MATTER
27, 13, 2700         * A, Z, Density [mg/cm3]
3, 2850             * Mode=3: Thickness in [mg/cm2], Thickness
0, 0, 0             * Geometry Mode 0: Homogeneous
0.0, 0.0, 0.0       * Shift in: x-direction, y-direction, angle
1, 1                * Toggle on/off: Scattering, E-stragglng
0, 0, 0, 0          * Matter thickness random mode, 0 = off

*****

```

Figure 5.9: *This card creates a section of matter with a certain extent in the z-coordinate. The first example shows how the list mode is used in combination with the thickness mode 2 [cm]. The second example shows the use of a standard material in combination with thickness mode 3 [mg/cm<sup>2</sup>].*

```

***** Wedge-Shaped Energy Degradr *****
WEDGE                * Starts the wedge specification
27, 13, 2700         * A, Z, Density [mg/cm3]
5370.0, -20.0, 0     * T_0, T_1, T_2
6                    * Mode = 6: Thickness in [mg/cm2]
1, 1, -1, 1         * Toggle/Choose: See below.
0, 0, 0, 0          * Thickness randomization, 0 = off

                    * Thickness = T_0 + T_1*X + T_2*X2
                    * Toggle: Small Angle Scattering, Energy
                    *           Stragglng, Momentum Distribution
                    *           of Fragments, Coulomb Scattering.

*****

```

Figure 5.10: *The WEDGE card defines a wedge shaped block of matter.*

A useful MOCADI tool for stopped beam experiments — and in all other cases the range of particles in matter is of importance — is the `STOP` card shown in Figure 5.11. This card stops all particles in a material defined by the user. If used before the `EXPECTED_VALUES` and/or `SAVE` card, (cf. Figure 5.13), the range of the ions reaching this position in the setup is written into the output files. The ion ranges in the defined material are given in  $\text{mg}/\text{cm}^2$ . For stopped beam experiments this card can be placed at the position of the stopper in order to see where particles are fully stopped in the material. Another useful application for this card is to put it after the production target, and setting the material to be aluminium, to get an idea about how much degrader one has to use to stop a specific isotope produced in the reaction.

```
***** Beryllium Stopper *****
STOP
9, 4                                * A, Z. The beam stops here and the remaining
                                      * flight length in the designated material
                                      * (Be 9) is calculated.
*****
```

Figure 5.11: *This command calculates the range of all particles at this position in the chosen material.*

### 5.2.5 Time of Flight

The time of flight of ions through the FRS is a parameter used for particle identification. In practice this clock is started and stopped by the signals from detectors, while MOCADI only needs a start signal and then keeps track of each particle's individual flight time since the start of that measurement. The card that starts the time of flight measurement is called `RESET` (see Fig. 5.12). The time of flight is also found in the output files, being zero at, and before the `RESET` card, and given in microseconds thereafter.

```
***** ToF *****
RESET                                * This starts the Time-Of-Flight clock.
*****
```

Figure 5.12: *The RESET card starts the time-of-flight clock.*

### 5.2.6 Saving

As illustrated in Fig. 5.13, saving in MOCADI can be done in two ways and with two different cards:

- **EXPECTED\_VALUES**: Summarises the characteristics of all particles passing this particular position in the setup. All important quantities,  $q$ , are included in this save, but it contains no information on individual particles, i.e., quantities are provided by isotope. All quantities are averaged and accompanied by the corresponding uncertainty by means of the standard deviation,  $\sigma_q$ . The **EXPECTED\_VALUES** card is the optimum way of saving to get a quick overview of the status at a certain position.
- **SAVE**: Using this card, MOCADI produces a HBOOK histogram output file, which can be used to plot the particles' characteristics at this position of the setup. The **SAVE** card keeps track of every individual particle and all its parameters, instead of averaging them like the in the **EXPECTED\_VALUES** case. The resulting save files can become very large, hence the **SAVE** card should only be used when absolutely necessary. Its contents can be plotted directly using for example PAW [18] or, after conversion of the output file, ROOT [19].

Both cards can be used in combination, and there can be many **SAVE/EXPECTED\_VALUES** cards in the same input file. Therefore, it is important to give all cards reasonable tags to make identification easy. Tagging is done by simply adding a string of characters after the card. The symbols '...' allow the tag to be more than one string of characters long, allowing for spacing. An example of this is shown in Fig. 5.13.

```
***** Expected Values *****
EXPECTED_VALUES          'Expected Values at Catcher'
SAVE                    SAVE#4_Catcher

                        * Creates an entry in the .out and .hbk file
*****
```

Figure 5.13: *These keywords save the properties of all passing particles in output files.*

### 5.2.7 Finishing the Simulation

All input files are concluded by the `END` card, which tells MOCADI to stop the simulation. Before this card, the `TABLE` card exemplified in Fig. 5.14, can be used to create a custom table with values from the `EXPECTED_VALUES` cards in the input file. The table will be found in an additional output file with the file extension `.tab`. If utilised properly, this function can save a great deal of time. Its function is similar to that of the `FRAGMENT` card (cf. Fig. 5.4). The parameter in the first line sets the number of table entries. The following lines contain one table entry each. Table entries have the form: `EXPECTED_VALUES` card number, desired quantity. For example: If the quantity of interest is the mean energy of a fragment at the position of the fourth `EXPECTED_VALUES` card in the input file, the entry should be 4, 5. The online MOCADI manual [15] contains a complete list describing which numbers to use for calling different quantities in the `TABLE` environment.

```
***** General Table *****
TABLE                               * The TABLE card outputs a user defined table
4                                   * Number of entries in the table
2, 1                               * EXPECTED_VALUES card 2, x-position
2, 101                             * EXPECTED_VALUES card 2, sigma_x
3, 5                                * EXPECTED_VALUES card 3, energy
3, 14                              * EXPECTED_VALUES card 3, Brho
*****
```

Figure 5.14: *The TABLE card defines a custom table.*



## 5.3 Output Files

All vital information needed for the preparation of an experiment at the FRS can be extracted from the `.out` files created by the `EXPECTED_VALUES` card. For an example of what a part of these files can look like, I refer to Fig. 5.15. Before the expected values are listed, there is a list of all components in the beamline, followed by a short summary list on all isotopes simulated. This list contains the fragment ID number, which serves as an additional fragment identifier in the expected values part of the output file. The expected values list is sorted by the fragment ID numbers, and within the fragment ID numbers by the  $z$ -value, i.e. the position of the save in the simulation.

Many of the in Fig. 5.15 listed parameters are self-explanatory, while some others may be not:

- **tr: teilchen** This value stands for 'transmitted particles', i.e. the number of particles of that specific isotope reaching this position in the FRS, out of the number of initial particles created in the production target. Hence this number should be compared to the number of beam particles (cf. Fig. 5.2), as explained in section 5.2.2. There are no reaction losses included in the `tr:teilchen` value.
- **wi: teilchen** This only difference between the `tr:teilchen` value and the `wi:teilchen` value is the fact that reaction losses are included in the latter.
- **tr: opt** This is the pure 'optical transmission' of the ions of this isotope. The value is normalised to the number of beam particles defined in the `BEAM` card (cf. Fig. 5.2).
- **tr: total** Normalised to the number of beam particles (cf. Fig. 5.2), this value gives the total particle transmission, taking into account reaction losses.
- **< nf/nsf >** This number is the ratio between the total number of fragments and the number of surviving fragments, i.e. the number of fragments which were not destroyed by secondary reactions in matter.
- **< delta e >** This value corresponds to the energy loss of the ions of this isotope since the previous `EXPECTED_VALUES` card. This comes in handy when the energy loss in detectors is of interest. For this purpose insert an `EXPECTED_VALUES` card before and after the detector or detector gas, run the simulation, and check the latter `EXPECTED_VALUES` card's `< delta e >` value.

The number of particles at any given position in the simulation are not corrected for reaction cross sections. Hence, plotting the results obtained from the `SAVE` card can give confusing results. However, the yield parameter in the output file gives the true production rates in the unit particles per incident projectile particle. In this parameter, losses due to secondary reactions and transmission efficiency are included. Hence the yield parameter should be multiplied with the number of beam particles in order to correct for production cross sections and losses in the FRS.

```

***** erwartungswerte 9 *****
(Expected_Values_Catcher)

i_fragment = 1
tr: teilchen = 5436 wi: teilchen = 3159.521 ( 3159.521)
tr: opt = 0.5436 tr: total = 0.315952
yield = 0.000598554 particle/incident particle
z = 7473.0306cm

< x >= -5.705160e-02 cm sigma x = 1.865107e+00 cm
max x = 6.653097e+00 cm min x = -8.498872e+00 cm

< a >= -2.733379e-02 mrad sigma a = 1.692549e+01 mrad
max a = 6.240895e+01 mrad min a = -6.244388e+01 mrad

< y >= -2.729603e-02 cm sigma y = 1.641121e+00 cm
max y = 6.011796e+00 cm min y = -5.822702e+00 cm

< b >= -2.587258e-01 mrad sigma b = 1.612978e+01 mrad
max b = 5.522762e+01 mrad min b = -6.487135e+01 mrad

< energie >= 4.551947e+01 Mev/u sigma energie = 7.202437e+00 Mev/u
max energie = 7.482261e+01 Mev/u min energie = 2.591244e+01 Mev/u

< time >= 3.491146e-01 mu s sigma time = 1.071370e-03 mu s
max time = 3.521892e-01 mu s min time = 3.450192e-01 mu s

< mass >= 5.393961e+01 u sigma mass = 7.127354e-06 u
max mass = 5.393961e+01 u min mass = 5.393961e+01 u

< z >= 2.600000e+01 sigma z = 0.000000e+00
max z = 2.600000e+01 min z = 2.600000e+01

< electrons >= 0.000000e+00 sigma electrons = 0.000000e+00
max electrons = 0.000000e+00 min electrons = 0.000000e+00

< nf/nsf >= 5.812216e-01 sigma nf/nsf = 2.906984e-03
max nf/nsf = 5.867720e-01 min nf/nsf = 5.690543e-01

< tof-tim >= 1.907058e-01 mu s sigma tof-tim = 9.204448e-04 mu s
max tof-tim = 1.936761e-01 mu s min tof-tim = 1.875477e-01 mu s

< delta e >= 2.455303e+03 Mev sigma delta e = 3.884966e+02 Mev
max delta e = 4.035903e+03 Mev min delta e = 1.397707e+03 Mev

< brho >= 2.033681e+00 Tm sigma brho = 1.639265e-01 Tm
max brho = 2.635032e+00 Tm min brho = 1.530991e+00 Tm

< range >= 5.327285e+01 mg/cm**2 sigma range= 1.392409e+01 mg/cm**2
max range = 1.195984e+02 mg/cm**2 min range = 2.133223e+01 mg/cm**2

```

Figure 5.15: An example of an output file. This part corresponds to an EXPECTED\_VALUES card placed right after the STOP card.

## 5.4 A MOCADI How-To

After the description of the program, its building blocks, and how to extract information from the output files, this section focuses on how to fit the pieces together to create a setting for a FRS experiment.

### 5.4.1 Getting Started

The first step should always be to obtain an appropriate input file to modify for your purpose, instead of creating one from scratch. This saves both time and insures that the drift lengths for the ion optical setup are most likely correctly implemented. In addition, it is helpful to use an input file which already contains different components that also will be used in your simulations. Different standard input files can be downloaded from the MOCADI homepage [15]. Although these files only are sparsely commented, they certainly contain the correct drift lengths. For the simulation of the FRS, a fully commented sample file can be downloaded from my homepage [17].

Once an appropriate file has been obtained, there are several things that should be checked and modified before the first simulation is run.

A good idea is to create an input file without optics first. This is easily achieved by, for example, commenting out all optical elements with the block comment command. This will make calculations much faster and still yield most of the later required parameters. The fine-tuning of the optics is done in the last steps of the creation of a setting. Before that, the optics will not be needed.

#### Initialisation & Beam

First of all, make sure the initialisation of the input file fits your needs. Specify the directory where the matrix files for the ion optics are stored and carefully search and replace all the matrix file names in the input file. Next, the **BEAM** card should be filled out. Set the number of beam particles to 10000 to get a quick start. If needed, this number can always be increased for better statistics later on. Define the primary beam particles, their mass, and their energy.

#### Target & Fragments

In the **TARGET** card, which should be located right after the SIS vacuum window and the SEETRAM in the case of the FRS, set the parameters to resemble the target of your choice. There is an online listing [10] of the different standard targets at the FRS and their properties. Also insert the properties of the setting fragment. If the target of choice incorporates a stripper foil, add a **MATTER** card that describes the stripper foil after the target. When this is done, the **FRAGMENT** card has to be checked and modified. During the first steps of the setting process, this list should be either empty or commented out of the code in order to save time. If it is already clear which fragments you want to simulated in addition to your setting fragment, insert these into the **FRAGMENT** card and then comment it out until later. Once this is done the settings for the target area of the FRS are finished.

### Slits & Scintillators

When creating a matter-only file, make sure all optical building blocks, including slits and collimators, are commented out. The next element in the beamline should then be found at the second focal plane of the FRS, the so-called S2 area. There are usually three components to be found there: a slit, a plastic scintillator and the wedge. Open the slit by setting its values to  $-100, 100, -100, 100$  and check if the scintillator thickness is correct. If the experiment has a time-of-flight measurement which incorporates the S2 scintillator, put the **RESET** card here.

### Wedge

To get an idea about how thick the wedge should be, one can follow a rule of thumb, which says that the wedge thickness in  $[\text{mg}/\text{cm}^2]$  should be about half of the setting fragment's range in aluminium after passing the target. To obtain this value, put a **STOP** card with the parameters 27, 13 after the **TARGET** card. This **STOP** card should be followed by an **EXPECTED\_VALUES** card and the **END** card, which marks the end of the simulation. Run MOCADI with this input file, check the newly created `.out` file for the range value of your setting fragment and insert the appropriate wedge thickness before removing the **STOP** and **END** cards again. The angle of the wedge can be easily calculated with LISE++ [16] or the **WEDGE** program [15], which is described on the MOCADI homepage. MOCADI uses the unit  $[\text{mg}/\text{cm}^2]$  to set the wedge angle. LISE++ will express the angle in the unit mrad. To convert it to  $\text{mg}/\text{cm}^2$ , this value should be multiplied by  $-2.700 [\text{mg}/\text{cm}^2/\text{mrad}]$ . However, be warned that the LISE++ wedge angle has the opposite sign due to different conventions. In general, using a thicker wedge gives better separation, but worse total transmission. For a thinner wedge it is the other way around. This concludes the S2 setting.

### The S4 Area

After the wedge the next section of ion optics follows. This should either be removed or commented out for the purpose of creating a matter-only file. The first element of a S4 setup is a vacuum window, which closes the beam pipe. After this there can be a wide variation of components in the setup depending on which type of experiment is run. The sample file [17] contains an example of the S4 setup that was used during the RISING Stopped Beam Campaign. The individual detectors used are usually the same, but their positions may vary. Special detectors, which are not FRS standard, have to be implemented carefully with **MATTER** and/or **DRIFT-IN-GAS** cards like the standard detectors in the sample file. At the end of the setup, put an **END** card to stop the simulation of particles there.

### Positioning Expected Values

Placing **EXPECTED\_VALUES** cards in appropriate places is important for being able to extract as much useful information from the output files as possible. Recommended positions are:

- After the target or stripper foil, if there is any.
- Behind the S1 slit.

- Before the S2 slits and after the wedge.
- Behind the S3 slit.
- After the exit window of the FRS at S4.
- At reasonable positions in the S4 setup. For example at the scintillator that triggers the time-of-flight measurement.

Giving the `EXPECTED_VALUES` cards sensible names will speed up later work. Once all this is done, it is time to run the simulation.

### Running the Matter-Only Input File

With the ion optics commented out in the input file, this simulation gives us the fragment energy at certain positions in the FRS, as well as the  $B\rho$  values of the setting fragment. The important values which should be noted are:

- The energy of the setting fragment after the target (and stripper), as well as the corresponding  $B\rho$  value.
- The energy of the setting fragment after the wedge and the corresponding  $B\rho$  value.

#### 5.4.2 Calibrating the Optics and Eliminating Errors

The energy of the setting fragment after the target is used as calibration energy for all optical building blocks between the target and S2. This can easily be achieved by doing a search and replace of the calibration string of the `MATRIX` cards' second line: A, Z, E. This procedure has the effect, that the setting fragment now will be centered throughout the FRS, when the ion optics are included in the simulation. Including the optics is the next step.

After running MOCADI with the full ion optical system included in the input file, check the position of the setting fragment throughout the FRS. It should be centered, i.e. never more than a few millimeters off center. If it is not centered, scale the magnets by slightly changing the calibration energy of the responsible ion optical blocks of the FRS until the setting fragment is centered. If the setting fragment does not show up at all, or is far off center, follow it through the FRS looking at the `EXPECTED_VALUES` output at different positions to locate the mistake. Possible sources of errors are:

- A slit in the beamline is partially or completely closed. Check all slits.
- Due to some error, there is too much matter in the beamline for the fragments to be able to penetrate. Check all cards comprising matter for thickness and element errors.
- The calibration line of one or several optical-building-block matrices contains errors, for example: the wrong mass number or energy was supplied. Check all optical blocks and check if the collimators have appropriate settings. The `COLL`

card is bugged in MOCADI 3.0c and may not have any comment or other string of characters behind it.

With the setting fragment centered throughout the FRS, it is appropriate to now include other fragments of interest in the simulation. Fragments you want to be sure of seeing should never travel more than approximately 10 cm off center. This is due to the acceptance of the FRS, the extent of the beamline, the S2 scintillator, and the wedge.

### Setting Slits & Fine-Tuning

At this point, the FRS setting is almost completed. However, there is one more important aspect to be considered: the count rate at different positions of the FRS. In order to reduce a high count rate ascribed to unwanted fragments or charge states, the use of slits has proven to be crucial. The most effective cuts can normally be achieved with the S1 slit.

The fine-tuning of the setting largely depends on the type of experiment to be simulated, but it most certainly comprises tuning of the slit and degrader settings, as well as the ion optics to optimise transmission efficiency and fragment separation.

### 5.4.3 Important Parameters for the Experiment

When the setting is fine-tuned and finally finished, the most important parameters for this setting of the experimental setup are:

- The beam energy and the target number, obtained from the GSI target list [10].
- The setting fragment's  $B\rho$  values and energies for all sections of the FRS.
- All degrader settings such as thicknesses and angles.
- All slit settings. Remember the sign change in the  $x$ -coordinate.

Additional information that can prove to be important are the positions of the fragments at S2 and S4, the approximate yields of different isotopes and other parameters that depend on what goals the experiment has. For a stopped beam experiment this would be, for example, the implantation depth of different isotopes in a stopper of a certain material.

## 5.5 LISE++

The windows program LISE++ [16] provides the user with an intuitive graphical interface to run simulations of modern fragment separators with user defined settings. A setup is built in a similar way as in MOCADI, stacking building blocks describing matter, drifts, and optical elements. Running a simulation with a certain setting of a fragment separator is done directly in the program by choosing one or several isotopes to be calculated. The results of the simulation can be displayed in a large variation of different useful default plots, in which the ion distributions automatically are calculated with a Monte Carlo code and instantly visualised. A brief overview is given in the three following sections. A LISE++ sample file can be downloaded from my homepage [17]. This file contains the whole FRS setup as it was used during the RISING Stopped Beam Campaign.

### 5.5.1 Building a Simulation

There are several predefined fragment separators in the program, among them is the FRS. The predefined setup of the FRS includes only the basic components such as a wedge and the ion optics, but can be easily modified if required. The included ion optical setup is fully tunable, while detectors and other layers of additional matter are not predefined and have to be added manually. This is done by defining new 'cards' in the 'Spectrometer Designing' option accessed via the 'Set-Up' button located at the upper left corner of the program window. Here, the user can choose from different kinds of building blocks, define their parameters and their positions. When the setup itself is built, it is appropriate to define certain materials in the setup to serve as detectors. This is done in the 'Plot Options' menu. For example, a plastic scintillator in the setup could be set to give the positions of the fragments, while an ionisation chamber yields the charge of the fragments by means of differential energy loss.

### 5.5.2 Creating a Setting

To create an experimental setting in LISE++ is much faster than in MOCADI. All parameters of the setting can be adjusted in the listing of setup components on the left side of the program window. First in this list are the Projectile, Fragment, Target, and Stripper cards. When everything is built and the basic parameters set, the 'Calculate the spectrometer for setting ion' button sets the optics to center the setting fragment throughout the FRS. In the component list to the left, the  $B\rho$  of the new setting fragment will be displayed for each dispersive element. The wedge setting can be tuned by accessing it from the component list. Here the program can calculate and set appropriate wedge angles for both achromatic and monochromatic mode. As mentioned in section 5.4, the output wedge angle is correct in the parameterisation used by LISE++, but has the opposite sign in the parameterisation of the FRS. After changing any setting, the 'Calculate the spectrometer for setting ion' button should be pressed in order to center the setting fragment again. Shifting the fragment positions can be done by scaling the  $B\rho$ -values of the dispersive elements

in the component list, similar to the procedure described in section 5.2.3 for MOCADI.

### 5.5.3 Running a Simulation and Plotting the Results

A simulation is simply run by clicking on one of the lightning marked buttons in the top menu bar. The most convenient way of choosing fragments is to define an area of fragments to be calculated in the nucleic chart. Once this is done – and it has to be redone in case of modified parameters in the setting – simply press the 'P-lightning' marked button to recalculate the previously calculated area in the nuclidic chart again. The output of a simulation are the yields and optical transmissions of the different isotopes inside the designated rectangle. All other information can be obtained by plotting the results of the simulation, using the different predefined plot types accessed through the plot icons on the left hand side of the top menu bar. The user can access additional helpful one- and two-dimensional plots from the respective drop-down menus. Figure 5.16 is an example of a predefined two-dimensional plot.

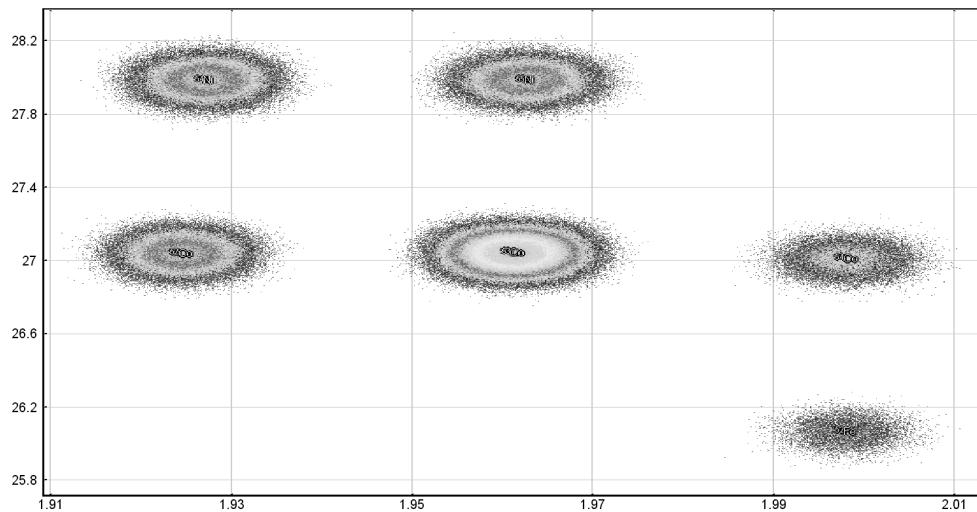


Figure 5.16:  $Z$  as a function of  $A/Q$  for the  $^{54}\text{Ni}$  setting, calculated by *LISE++*'s Monte Carlo code. The "blobs" seen in the picture are the ion distributions of  $^{54}\text{Ni}$  (upper left),  $^{55}\text{Ni}$  (upper center),  $^{52}\text{Co}$  (left),  $^{53}\text{Co}$  (center),  $^{54}\text{Co}$  (right),  $^{52}\text{Fe}$  (lower right).



# Chapter 6

## Results

In this section I will present the results of the simulations I created in the process of preparing the  $^{54}\text{Ni}$  fragmentation experiment, described in chapter 3, which is utilising the experimental setup delineated in chapter 4. Different settings were created for the purpose of FRS calibrations and production runs. The calibration settings will be summarised in section 6.1, and three production settings in sections 6.2–6.4.

The general features of the settings are:

- The primary beam is  $^{58}\text{Ni}$  with a SIS energy of 550 MeV/u.
- Two different targets are used. A 1032 mg/cm<sup>2</sup>  $^9\text{Be}$  target for the  $^{54}\text{Fe}$  and  $^{54}\text{Ni}$  setting, and a 4007 mg/cm<sup>2</sup>  $^9\text{Be}$  target for the  $^{43}\text{V}$  setting.
- Scintillator 21 has a thickness of 3.37 mm in all experiments.
- The S4 setup, described in section 4.2, is identical in all settings, with one exception. The stopper used in the  $^{54}\text{Fe}$  and  $^{54}\text{Ni}$  experiment is a 4 mm thick Be plate, while the stopper used in the  $^{43}\text{V}$  experiment is a 12 mm thick plastic stopper. A parameter that varies in the different production settings is the S4 degrader thickness.

### 6.1 Calibration Settings

All calibrations are done with a low intensity primary beam and progressively more elements in the beam line. In all settings, the primary beam is centered throughout the FRS. The settings required for the calibration of the experimental setup are:

1. **Beam-Through Setting:** There is no matter in the beamline except for vacuum windows and thin particle detectors like the SEETRAM and Multiwire detectors.
2. **Beam-Through Sci21 Setting:** Scintillator 21 is added to the beamline.
3. **Target Sci21 Setting:** The 1032 mg/cm<sup>2</sup>  $^9\text{Be}$  production target is inserted and the beam recentered.

4. **Four Wedge Settings:** The wedge shaped energy degrader is added to the beamline. Four settings that comprise different wedge thicknesses are created. The production wedge setting No. 4.2, one setting with a thinner wedge and two settings with a slightly thicker wedge than in the production wedge setting.

The most important parameters obtained from these simulations are listed in Table 6.1. The 'Setting No.' corresponds to the listed items above. For more details on the calibration process I refer to section 7.1.

Table 6.1: Calibration Settings – predicted setting parameters.

| Setting No.<br>Unit | S1 $B\rho$<br>[Tm] | Wedge<br>[mg/cm <sup>2</sup> ] | S3 $B\rho$<br>[Tm] | MUSIC41 $\Delta E$<br>[MeV] | S2-S4 ToF<br>[ns] |
|---------------------|--------------------|--------------------------------|--------------------|-----------------------------|-------------------|
| 1                   | 7.9478             | 0                              | 7.9478             | —                           | —                 |
| 2                   | 7.9478             | 0                              | 7.7878             | —                           | —                 |
| 3                   | 7.6724             | 0                              | 7.5553             | —                           | —                 |
| 4.1                 | 7.6724             | 4500                           | 6.1970             | 326.6                       | 179.9             |
| 4.2                 | 7.6724             | 5300                           | 5.9118             | 341.0                       | 184.5             |
| 4.3                 | 7.6724             | 5800                           | 5.7230             | 351.8                       | 187.8             |
| 4.4                 | 7.6724             | 6500                           | 5.4425             | 370.0                       | 193.2             |

## 6.2 <sup>54</sup>Fe Setting

The first production setting in the <sup>54</sup>Ni experiment is meant to check whether the experimental setup is working properly. This is achieved by monitoring the well-known isomeric 10<sup>+</sup> state in <sup>54</sup>Fe. A very high intensity secondary beam is easily produced because of the favourable "α-like" removal required for the production of <sup>54</sup>Fe with the <sup>58</sup>Ni beam. The setting is supposed to be as clean as possible to ensure a maximum rate at which good statistics are acquired. For this reason components in the beamline are set as described in Table 6.2. All slits not mentioned in the table are opened completely. Other important parameters are given in Table 6.3

It is necessary to close the S1 slit completely on the high momentum side of the ion distributions to prevent that the primary beam, located at approximately +7 mm at the S1 slit, reaches the S2 setup. Hence, one half of the <sup>54</sup>Fe ion distribution must be cut. This is not a problem because of the very high <sup>54</sup>Fe yield. The setting is highly limited by the S4 rate, i.e. the maximum possible yield of <sup>54</sup>Fe at S4 exceeds the maximum rate of particle identification. To reduce this effect, the S3 and S4 slits could be used to cut unwanted ion distributions. However, we chose to keep the setting as simple as possible and, hence, no additional slits were used. The high-yield problem is easily solved by decreasing the primary beam intensity to a degree that results in a maximum possible S4 rate.

The wedge thickness and angle is set to be the same as in the <sup>54</sup>Ni production setting. This can be done without losing too much secondary beam quality because

of the relatively small difference between the  $^{54}\text{Fe}$  and  $^{54}\text{Ni}$  fragment. The wedge angle does not change significantly when optimised for the respective fragment. This allowed us to quickly switch between the  $^{54}\text{Fe}$  and  $^{54}\text{Ni}$  production setting.

What is significantly different in the  $^{54}\text{Fe}$  setting as compared to the  $^{54}\text{Ni}$  setting is – except for the  $B\rho$  values – the S4 degrader setting. Having two protons less than  $^{54}\text{Ni}$ ,  $^{54}\text{Fe}$  loses less energy in the same amount of matter. MOCADI and LISE++ simulations agree, that the optimum S4 degrader thickness should be set to 4750  $\text{mg}/\text{cm}^2$ . This thickness implies that the  $^{54}\text{Fe}$  ions have an average energy of 50  $\text{MeV}/\text{u}$  before implantation in the  $^9\text{Be}$  stopper.

Table 6.2: The  $^{54}\text{Fe}$  beamline setting.

| Setting Unit           | S1 Slit [cm] | S1 $B\rho$ [Tm] | Wedge [ $\text{mg}/\text{cm}^2$ ] | Wedge Angle [mrad] | S3 $B\rho$ [Tm] | S4 Degrader [ $\text{mg}/\text{cm}^2$ ] |
|------------------------|--------------|-----------------|-----------------------------------|--------------------|-----------------|---|
| $^{54}\text{Fe}$ Prod. | -100, 0      | 7.6950          | 5300                              | 7.1512             | 6.109           | 4750                                    |

Table 6.3: Characteristics of the  $^{54}\text{Fe}$  setting.

| Setting Unit           | S1 E [MeV/u] | S1 $\beta$ [v/c] | S3 E [MeV/u] | S3 $\beta$ [v/c] | MUSIC41 $\Delta E$ [MeV] | ToF [ns] | S4 x-Pos [cm] |
|------------------------|--------------|------------------|--------------|------------------|--------------------------|----------|---------------|
| $^{54}\text{Fe}$ Prod. | 518.5        | 0.7663           | 351.8        | 0.6878           | 285.2                    | 181.5    | 0.2           |

## 6.3 $^{54}\text{Ni}$ Setting

The setting for the main experiment is optimised for two fragments:  $^{54}\text{Ni}$  and  $^{52}\text{Co}$ . Goals of this setting are:

- A good separation of the ion distributions.
- A maximum, clean S4 yield in which  $^{54}\text{Ni}$  dominates.
- As low as possible optical loss in the wings of the  $^{54}\text{Ni}$  momentum distribution.

To ensure these goals are reached, there are several issues that have to be considered. At a certain ion energy, measured in  $\text{MeV}/\text{u}$ , the 'sum' of all layers of matter needed to stop a specific ion is a constant. A higher beam energy means that more matter is needed to stop the ions. The more matter there is, the better the separation will be - within reasonable limits. At the same time, more matter gives broader momentum distributions and more reaction losses. The wedge-shaped energy degrader at S2 yields the ion distribution separation, and should be thick enough to give a large enough separation. If the wedge is too thick, the momentum distributions will become wider than the acceptance of the second part of the FRS. Ions will then be lost for ion optically reasons. Simulations have shown that a good compromise is to use a relatively low beam energy of 550  $\text{MeV}/\text{u}$ , a 1032  $\text{mg}/\text{cm}^2$   $^9\text{Be}$  target that almost completely avoids the loss of the momentum wings of the  $^{54}\text{Ni}$  ions in the first part of

the FRS, and a wedge thickness of  $5300 \text{ mg/cm}^2$ . Another advantage of the low beam energy is the relatively thin S4 degrader required to reduce the fragments' average energy to implantation energies, resulting in less radiation background produced as the ions pass the degrader. The implantation depths of the ions is displayed in Fig. 6.1.

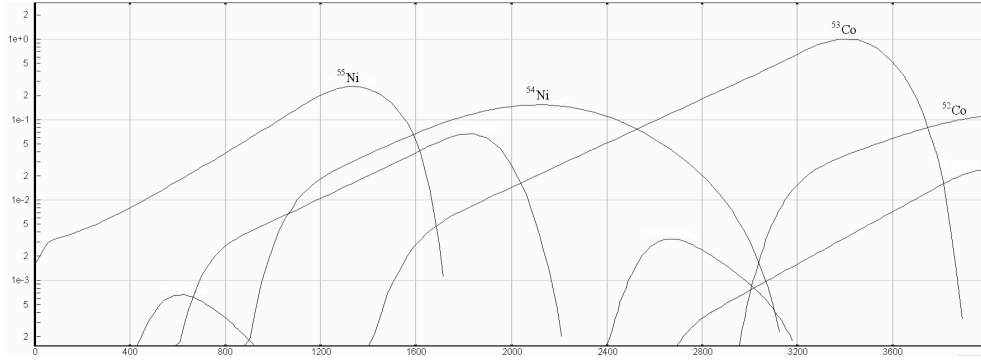


Figure 6.1: The relative number of ions of a specific species that is stopped, as a function of depth in the stopper. Calculated with LISE++.

These parameters given, an optical setting can be made. Simulations with MO-CADI and LISE++ show that the high S2 rate can be significantly reduced by cutting part of the distribution of ions with the S1 slit. Set to 25 mm at the high momentum side, most of the less exotic ions with high intensity are cut without losing any significant part of the  $^{54}\text{Ni}$  distribution. The results of the simulations are shown in Table 6.4.

Table 6.4: The  $^{54}\text{Ni}$  beamline setting.

| Setting                | S1 Slit  | S1 $B\rho$ | Wedge                | Wedge Angle | S3 $B\rho$ | S4 Degrader          |
|------------------------|----------|------------|----------------------|-------------|------------|----------------------|
| Unit                   | [cm]     | [Tm]       | [ $\text{mg/cm}^2$ ] | [mrad]      | [Tm]       | [ $\text{mg/cm}^2$ ] |
| $^{54}\text{Ni}$ Prod. | -100, 25 | 7.123      | 5300                 | 7.1512      | 5.320      | 2650                 |

To have both the  $^{54}\text{Ni}$  and the  $^{52}\text{Co}$  distribution stopped at the final focal plane of the FRS, the  $^{54}\text{Ni}$  ion distribution is shifted by about 4 cm in the second half of the FRS, moving the  $^{52}\text{Co}$  distribution 4 cm closer to the center of the stopper, placing it at -8 cm. The result of this shifting is seen in Fig. 6.2.

The  $^{54}\text{Ni}$  yield at the final focal plane in the simulations is approximately 1000 ions per spill. The  $^{52}\text{Co}$  yield is of the same order of magnitude and including a few contaminant isotopes like  $^{55}\text{Ni}$ ,  $^{53}\text{Ni}$ ,  $^{53}\text{Co}$ , and  $^{51}\text{Fe}$  that partially reach the final focal plane, the setting allows for a maximum beam intensity of  $5 \cdot 10^9$  particles per spill, while maximising the S2 and S4 rates for good statistics. Other important characteristics of the  $^{54}\text{Ni}$  setting fragment, and all other fragments reaching the final focal plane, are listed in Table 6.5. In this table, the Yield parameter is given in particles

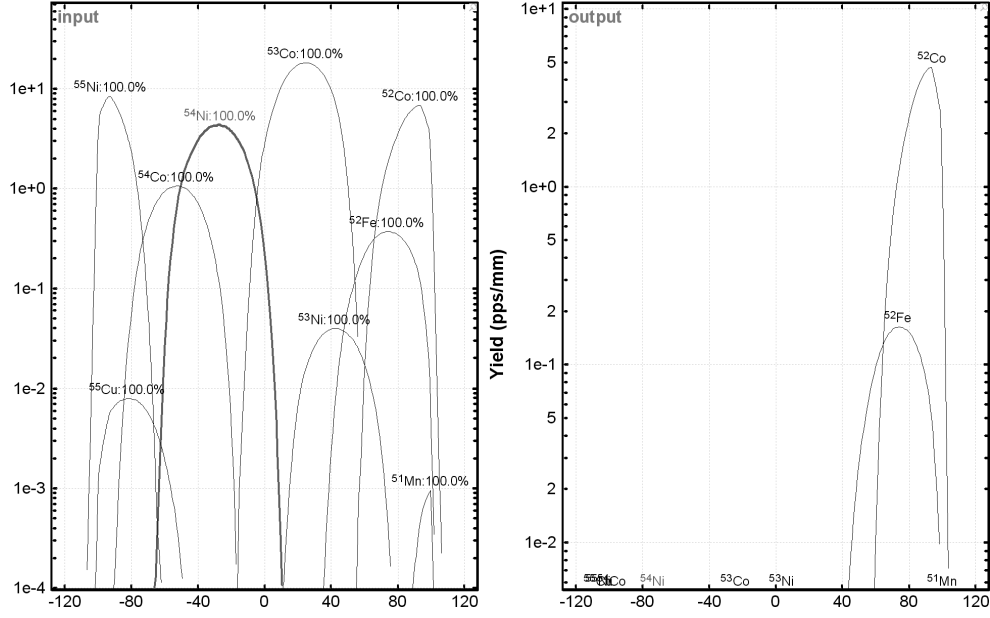


Figure 6.2: Relative intensity (logarithmic) as a function of  $S4$   $x$ -position as obtained from a  $LISE++$  calculation. The left plot shows the position and relative intensity of incoming ions at the stopper. The plot to the right shows the ions passing through the stopper without being stopped.

per incident particle, ppip, and the yields and particle positions are corresponding to a setting with all slits opened throughout the FRS. As mentioned above, when the  $S1$  slit is closed, the intensity of less exotic isotopes is highly reduced. The slit blocks most of the  $^{55}\text{Ni}$  and  $^{53}\text{Co}$  distribution, while  $^{51}\text{Fe}$  is taken out by the acceptance of the FRS in this case.

Table 6.5: Characteristics of the  $^{54}\text{Ni}$  setting

| Fragment<br>Unit | $S1$ E<br>[MeV/u] | $S3$ E<br>[MeV/u] | MUSIC41 $\Delta E$<br>[MeV] | ToF<br>[ns] | $S4$ x-Pos<br>[cm] | Yield<br>[ppip] |
|------------------|-------------------|-------------------|-----------------------------|-------------|--------------------|-----------------|
| $^{55}\text{Ni}$ | 516.9             | 306.4             | 357.9                       | 189.5       | +11.28             | 2.702E-07       |
| $^{54}\text{Ni}$ | 516.2             | 314.6             | 352.9                       | 188.0       | +3.86              | 2.353E-07       |
| $^{53}\text{Ni}$ | 515.5             | 323.5             | 347.3                       | 186.3       | -3.88              | 2.008E-09       |
| $^{53}\text{Co}$ | 516.7             | 314.8             | 327.5                       | 187.9       | -0.83              | 1.785E-06       |
| $^{52}\text{Co}$ | 516.1             | 323.3             | 322.6                       | 186.3       | -8.17              | 2.953E-07       |
| $^{51}\text{Fe}$ | 516.3             | 323.2             | 298.9                       | 186.2       | -12.18             | 1.102E-06       |

## 6.4 $^{43}\text{V}$ Setting

The  $^{43}\text{V}$  setting is different from the  $^{54}\text{Ni}$  and the  $^{54}\text{Fe}$  setting in many ways. Its aim is not the study of one or two particular isotopes, but rather to scan an *area* of the nuclidic chart for isomers. The following points summarise the goals of this experimental setting:

- The isotopes  $^{45}\text{Cr}$ ,  $^{44}\text{V}$ , and  $^{40}\text{Sc}$  should be inside the scanned area.
- A large number of additional isotopes should reach the final focal plane of the FRS, with ion distribution widths that allow for easy particle identification.
- The 'setting fragment' should be chosen in a way that gives a neither too high, nor too low S2 and S4 rate, and yet permit the study of proton-drip-line nuclei with reasonable statistics.

To incorporate all points into a setting that may produce new results within less than one day of effective beamtime, the first things one has to consider are what target, wedge, and S4 degrader settings give the best results. While a thin target gives only little additional separation and ensures small momentum distribution widths, it has the disadvantage of reducing the effective production rate through a lower production cross section. On the other hand, a thick target would give some additional, undesired separation and broader distributions, but also it would serve as an energy degrader. With a thin target and a thin wedge, which is required to permit a large area of the nuclidic chart can be covered, the S4 degrader would have to be very thick to be able to stop the ions. A thick degrader also implies a higher radiation background. Because of this, it is reasonable to choose a thick target, and the 4 g/cm<sup>2</sup>  $^9\text{Be}$  target proves to be the optimum for this purpose.

With this setting a large area of nuclei is covered: from  $^{47}_{25}\text{Mn}$  down to  $^{38}_{20}\text{Ca}$ , most of the exotic nuclei in this area are transmitted. Even though the thick target was chosen, one still needs a 4200 mg/cm<sup>2</sup> thick S4 degrader for proper implantation. The implantation of the different ions is not as easy as in the  $^{54}\text{Ni}$  case, because of the strongly varying proton number of the ions. To stop most of them, a much thicker or denser stopper than the 4 mm  $^9\text{Be}$  plate is needed. MOCADI and LISE++ simulations show that a 12 mm plastic stopper would stop all ions but the very light ones. A summary of the beamline setting with the most important parameters is given in Table 6.6.

Table 6.6: The  $^{43}\text{V}$  Beamline Setting

| Setting<br>Unit       | S1 $B\rho$<br>[Tm] | Wedge<br>[mg/cm <sup>2</sup> ] | Wedge Angle<br>[mrad] | S3 $B\rho$<br>[Tm] | S4 Degrader<br>[mg/cm <sup>2</sup> ] |
|-----------------------|--------------------|--------------------------------|-----------------------|--------------------|--------------------------------------|
| $^{43}\text{V}$ Prod. | 6.1781             | 2000                           | 2.8847                | 5.5154             | 4200                                 |

# Chapter 7

## The Experiment

The  $^{54}\text{Ni}$  experiment was the last in a series of three experiments during the RISING stopped beam campaign during February/March 2006. The campaign and the experimental setup has been outlined in Chapter 3 and 4. This chapter summaries the calibration process of the FRS and the involved detectors.

### 7.1 Calibrations

All FRS calibrations are made with a low intensity ( $\sim 10^3 - 10^4$  particles per spill) primary beam. A low intensity beam is required because of the very sensitive multi-wire detectors used to determine the position of the beam throughout the FRS. The concept of the FRS calibration can be summarised as having the primary beam centered throughout the FRS while adding progressively more matter into the beamline and recentering the beam each time matter has been added. As mentioned in section 5.2.3, this is done by scaling the magnetic fields of the ion optics by the correct amount. The most important ion-optical components for this procedure are the four dipole bending magnets in the setup. A higher dipole field strength bends the beam more than a low field strength, and all magnets can individually be set to a field strength that corresponds to a certain magnetic rigidity. The concept of magnetic rigidity was addressed in section 4.1.1. This procedure is an effective way of measuring the effective thicknesses of components such as scintillators and degraders in the setup.

A rough scheme of the different steps in the FRS calibrations is given in the following. An overview of the facilitating simulations resembling the steps below is given in section 6.1. The simulations turned out to be very accurate and the proposed settings only needed minor adjustments.

1. Initially a higher primary beam intensity, of  $10^7 - 10^8$  particles per spill, and the so-called current grids, mounted in front and behind the target, are used to check if the primary beam entering the FRS from the SIS synchrotron, is focused on the target and enters at zero angle.

2. Once the beam is centered correctly in the target area of the FRS, a beam-through setting can be created by utilising the results of the simulations performed prior to the start of the experiment. The  $B\rho$ -value of the beam is constant throughout the FRS due to the lack of matter between the target area and the FRS exit window.
3. The effective thicknesses of the production target and Sc21 are calculated. The scintillator is inserted into the beamline in the S2 area, and the magnetic rigidities in the second half of the FRS are rescaled to again center the beam. Then the production target is inserted into the beamline and the beam recentered. When this is done, the matter thicknesses in the first half of the FRS are calibrated.
4. The second half of the FRS is calibrated in two steps. The first step is to calibrate the MUSICs in the setup by varying the S4 beam energy through the variation of wedge degrader thickness. At the same time the effective wedge degrader thickness is determined. This process requires three or four different wedge degrader settings that produce appropriate primary beam energies at S4. 'Appropriate' in this case implies energies that yield energy losses in the MUSICs, at and around those of the setting fragment.
5. The second step is to calibrate the time of flight between the scintillators Sc21 and Sc41. To check the detector response over the whole detector area with the usually very focused primary beam, the last quadrupole magnet before the scintillator can be switched off. Then the defocused beam is slowly swept across the whole detector area by manually scaling the magnetic field of the last dipole magnet before the scintillator. This works for Sc21 as well as for Sc41. After this step the major steps of the calibration process are completed.
6. Not part of the primary beam calibrations is the setting of the S4 degrader for proper implantation of the setting fragment in the stopper. This can be rather tricky as one is very limited regarding the observables of a correct implantation. If the stopper is thick enough and the S4 degrader works correctly, accurate LISE++ and MOCADI simulations, taking into account *all* matter in the setup, are good enough to ensure a correct implantation. An alternative way of checking the implantation is to vary the S4 degrader thickness around a calculated value while observing the energy spectrum of the veto Sc43, gated on the desired fragment. If there is no signal, the S4 degrader could be too thick and prevent the ions from reaching the stopper. If there is a clean peak in the spectrum, (almost) all fragments pass right through the stopper. The desired spectrum would show only few Sc43 hits with a wide spread of low energies – this would imply that all fragments are stopped in the stopper except for those in the high momentum wing of the fragment momentum distribution.

Of course, there are many more calibrations involved in the set-up process of the experiment. Before any FRS calibrations are made, the electronics of the FRS detectors and the Germanium detector array are set up and calibrated by different means. As an example, the energy calibration of the array is done with a  $^{152}\text{Eu}$  calibration source for each individual detector crystal in the array. The gains and offsets are



set to match the known  $\gamma$ -ray energies. This serves as a coarse energy calibration that is good enough for all online and preliminary analysis. A more thorough energy calibration for later analysis is made with a low intensity  $\gamma$ -source, which provides lines in a wider energy range, to have an accurate energy-per-channel value over the whole spectrum.

## 7.2 Data-Run Summary

The  $^{54}\text{Ni}$  experiment was given a total of four days of beamtime, which we split into three different parts. The first two eight-hour shifts were dedicated to FRS calibrations and gathering data on the well known  $^{54}\text{Fe}$  isomer in order to check if the method and the setup is working properly. Due to the very high production cross section of the  $\alpha$ -like removal to produce  $^{54}\text{Fe}$  out of  $^{58}\text{Ni}$ , the primary beam intensity was set to around  $10^7$  particles per spill. This yielded the maximum possible S4 rate and thus, good statistics acquired within a short time.

The following seven shifts were used for  $^{54}\text{Ni}$  data runs. The experiment was run at a maximum possible primary intensity of approximately  $5 \cdot 10^9$  particles per 10-12 second spill. Initially the S4 degrader was set to the wrong value that caused all  $^{54}\text{Ni}$  ions to be stopped before reaching the stopper. The next problem became apparent shortly after: the particle identification through the  $A/Q$  measurement was smeared out and the time-of-flight measurement showed a poor resolution. This problem was not solved until some hours later, when the wedge angle,  $\theta$  was discovered to be set to  $-\theta$ . As this was corrected by resetting the wedge properties, the resolution improved significantly. The FRS setting was further optimised toward the transmission of  $^{54}\text{Ni}$ , when there were no isomers found in the secondary setting fragment  $^{52}\text{Co}$ . The last four shifts no further serious problems occurred.

After gathering enough statistics with the  $^{54}\text{Ni}$  data-runs, we switched to the  $^{43}\text{V}$  setting discussed in section 6.4. This had completely different characteristics than the  $^{54}\text{Ni}$  and  $^{54}\text{Fe}$  settings. It proved to be S4 rate limited and the primary beam intensity had to be reduced to about  $1 \cdot 10^9$  particles per spill. There were no complications during the two shifts this setting was run and considering the short time dedicated to this experiment, a good amount of statistics was collected.



## Chapter 8

# Preliminary Data Analysis

In this chapter I will briefly comment on some of the experimental data analysis done until the end of May 2006. The results presented here are preliminary and incomplete. They may undergo minor changes in a later, more thorough analysis. There may also more details to be found in the data. The first section of this chapter provides an overview of the concepts of the data analysis as well as its results, which will be discussed in section 8.2.

### 8.1 Concept

During the calibrations and data-runs, totally 120 GB of data was collected. The data consists of so-called events that are puzzled together by the electronics and software of the experimental setup. The information contained in these events is extracted by means of 'sorting' the events, i.e. building files containing the event information in a way that makes it directly accessible by a program that can produce histogram files and/or plot the contained information. Even though a raw, unfiltered spectrum in some cases can reveal some information, non-obvious details are not visible. To extract all hidden information, conditions (or "gates") must be put on the spectra. In the case of FRS experiments, these filtering conditions are primarily connected to the particle identification.

A gate or condition is simply a requirement that all registered particles in a specific data interval (one-dimensional gate) or area (two-dimensional gate), and the events they give rise to, are accepted, while all others are discarded. There are several spectra available for correct particle identification, the two most frequently used are the time of flight versus S4  $x$ -position and  $Z$  versus  $A/Q$ . To place gates in these two two-dimensional spectra is very effective to clean up, for example, a  $\gamma$ -ray energy spectrum. Taking a look at Fig. 5.16, placing a condition around the  $^{54}\text{Ni}$  "blob" would imply that an energy spectrum using this condition would show  $\gamma$ -ray lines from  $^{54}\text{Ni}$  only, possibly including some generic background. To use several conditions in different identification spectra at the same time can significantly enhance the visible detail in a spectrum gated by these conditions.

A two-dimensional energy-time matrix is used to picture the decays of isomeric states of ions implanted in the stopper. As long as the half-lives of isomers are long enough to outlast the "prompt flash", which is caused by ionisations and emission of bremsstrahlung during the implantation of the fragments in the stopper, isomeric decay will become visible as soon as the strong initial background radiation has died out. Figures 8.1 and 8.2 show gated  $E_\gamma$ - $t_\gamma$  matrices for the decay of the stopped  $^{54}\text{Ni}$  ions. The vertical high intensity band seen in these spectra is the flash. Clearly visible are the horizontal lines, which are either natural background radiation,  $\gamma$  rays from  $^{\text{nat}}\text{Ge}(n,\gamma)$  reactions in the detector crystals, or the wanted  $\gamma$  rays from isomeric decays. The natural background lines are easily detected as they have a constant intensity at all times. Isomers are seen as horizontal lines of decreasing intensity as time increases.  $\text{Ge}(n,\gamma)$ -lines have a similar look, but can be identified as non-isomers, because these are transitions with well known energies.

Further analysis of the energy-time matrices incorporates the creation of projections. To get a clean energy spectrum that contains mostly  $\gamma$ s from isomeric decay and little background radiation, the prompt flash is cut away by selecting an appropriate time interval containing the isomers and as little background radiation as possible. A projection of this data onto the energy axis then gives a much cleaner picture of the transitions than a projection including the flash would give. A projection of the  $^{54}\text{Ni}$  data is displayed in Fig 8.3.

There are several delayed decays observed in Fig. 8.3(a), which is Ni-gated but not background subtracted. Except for several easily identified low intensity natural background lines, both a prominent 511 keV peak from positron annihilation, and  $\text{Ge}(n,\gamma)$  lines are observed. As these lines always are present in this experimental setting, and are independent of what particle identification gates are used as filters, they disappear once the background is subtracted. An appropriate background spectrum for subtraction is obtained by gating on Co,  $Z = 27$ , which shows no signs of any isomeric decays, and thus is a "pure" background radiation spectrum that contains both the flash from the implantation, and the generic background radiation. Once properly scaled by a factor to match the background intensity of the  $Z = 28$  gated spectrum, and subtracted from the latter, a set of seven clean peaks emerges in Fig 8.3(b).

To determine the lifetimes of observed transitions, a projection onto the time axis is created. By choosing a suitable energy interval, and projecting the data onto the time axis, an exponential decay becomes visible. To extract the lifetimes from this data, an exponential function of the form  $y(t) = A_0 \cdot e^{-A_1 t} + A_2$  can then be fitted to the data, where  $1/A_1$  gives the lifetime,  $\tau$ , of the isomer.

The analysis of the isomeric lifetimes is not as straight forward as one would imagine. Taking a look at Fig. 8.4, the dilemma of choosing an appropriate time interval for a linear regression becomes evident. Also the amount of statistics in each channel has to be considered, as the unweighted method in this case is prone to large uncertainties when considering a time interval with low statistics. Using an unweighted least mean square fit, a 100 ns shift in fitting interval yields differences in lifetime results of up to 30 ns, even though the fitting is done in a beforehand accepted time

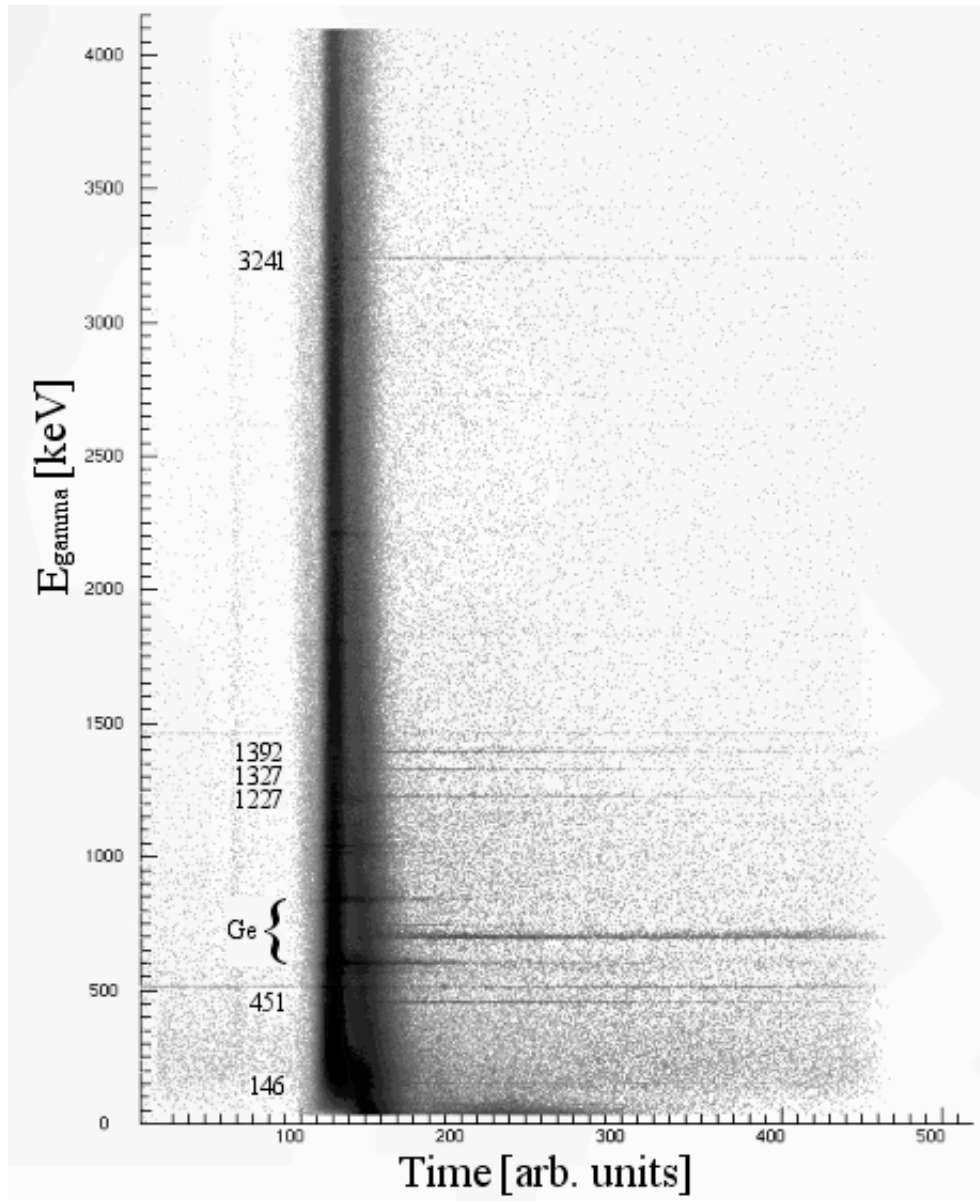


Figure 8.1: The  $\gamma$ -ray energies as a function of short-range TDC time. The TDC was set in software to have a resolution of 2.4 ns per channel. Clearly visible are several  $^{54}\text{Ni}$  lines which are part of the cascade down to the nucleus' ground state. These lines are here given numbers that correspond to the energy of the transitions, measured in keV. Several lines from nuclear reactions in the germanium crystals are marked by the parenthesis.

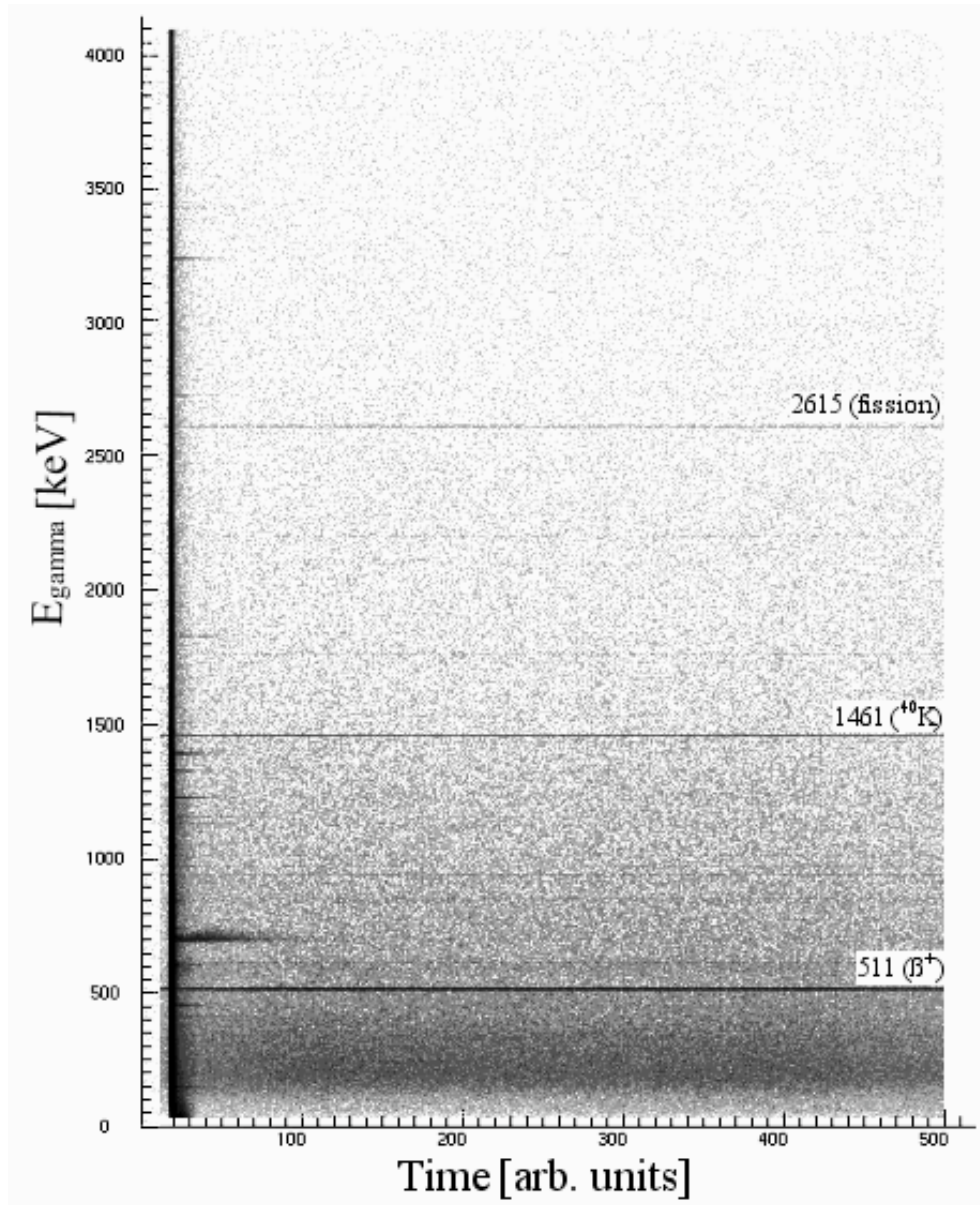


Figure 8.2: The  $\gamma$ -ray energies as a function of long-range TDC time. The TDC was set to have a resolution of about 40 ns per channel. In this plot the natural background radiation becomes more evident. The two most prominent natural background lines are the 1461 keV  $^{40}\text{K}$  line and the 2615 keV line from the  $\gamma$ -decay of  $^{208}\text{Pb}$  as the last step in the Th-decay chain. The 511 keV line, which derives from the annihilation of positrons, is constantly present due to the  $\beta^+$  decay of the neutron deficient nuclei involved in the experiment.

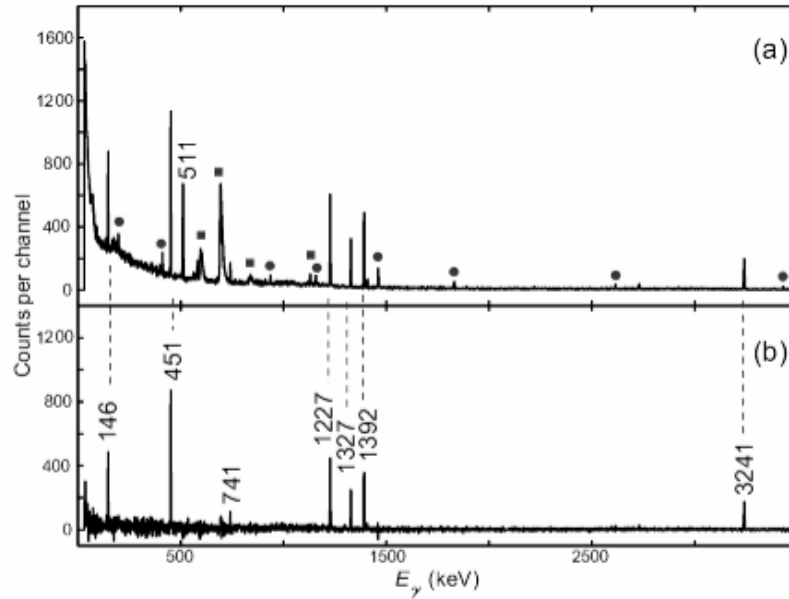


Figure 8.3: Energy spectra of  $^{54}\text{Ni}$  in the time interval 110 ns – 510 ns. (a) Channel 23–33 of the long-range TDC, gated by  $Z = 28$ . Solid circles mark background peaks of contaminants and natural decays, while the squares mark Ge-lines. (b) A background subtracted version of (a). The background is obtained from a  $Z = 27$  gated version of the energy-time matrix.

interval. As a consequence of this, the actual uncertainty of the fit should be considerably larger than the calculation suggests. Weighted by the square root of counts in each channel of the long range TDC data (channel 24 to 37), a fit is displayed in Fig. 8.5.

The above methods of analysis render the characteristics of the observable transitions, but do not explicitly prove that the observed transitions are connected as parts of the same cascade down to the ground state. This can be proven with a so-called  $\gamma - \gamma$  matrix, which highlights all transitions that are registered simultaneously or within a short time interval. Excluding the prompt flash and setting appropriate conditions, a  $\gamma - \gamma$  matrix can display all  $\gamma - \gamma$  coincidences, given enough statistics. Three differently gated projections of the  $^{54}\text{Ni}$   $\gamma - \gamma$  matrix are presented in Fig. 8.6.

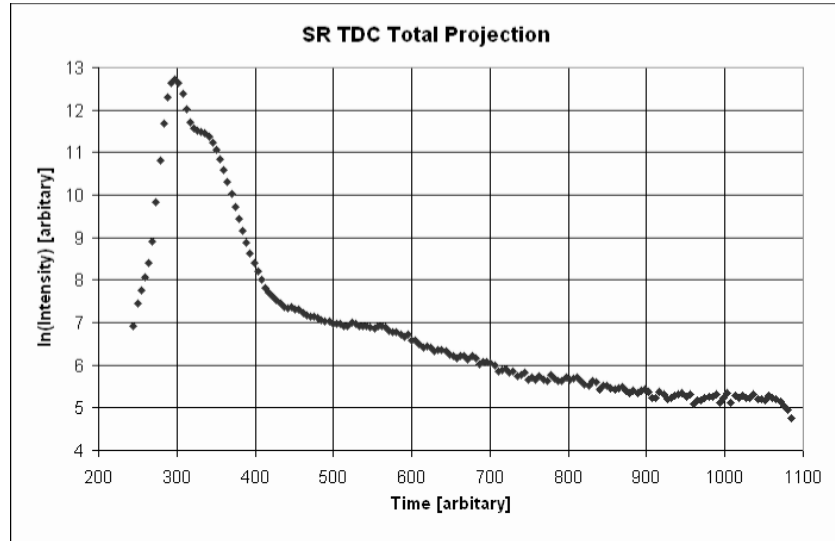


Figure 8.4: The logarithmic intensity variation of the sum of all  $\gamma$  rays as a function of the time provided by the short-range TDC. During the flash the intensity reaches its maximum and rapidly decreases thereafter, fading into a mixture of isomer  $\gamma$  rays and remnants of the flash. Later the isomer decay blends with the constantly present background radiation.

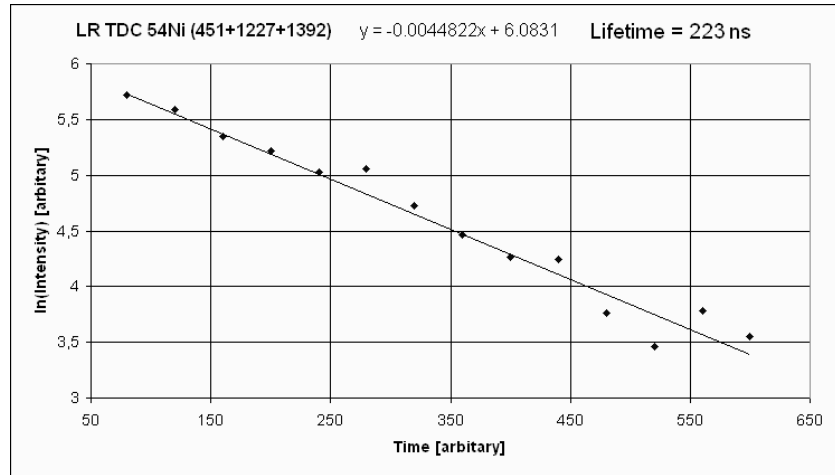


Figure 8.5: The logarithmic intensity as a function of the long range TDC time. A weighted linear regression is represented by the fitted line, and its equation is shown in the figure. The obtained value for the lifetime of the  $^{54}\text{Ni}$  isomer is  $\tau = 223$  ns.



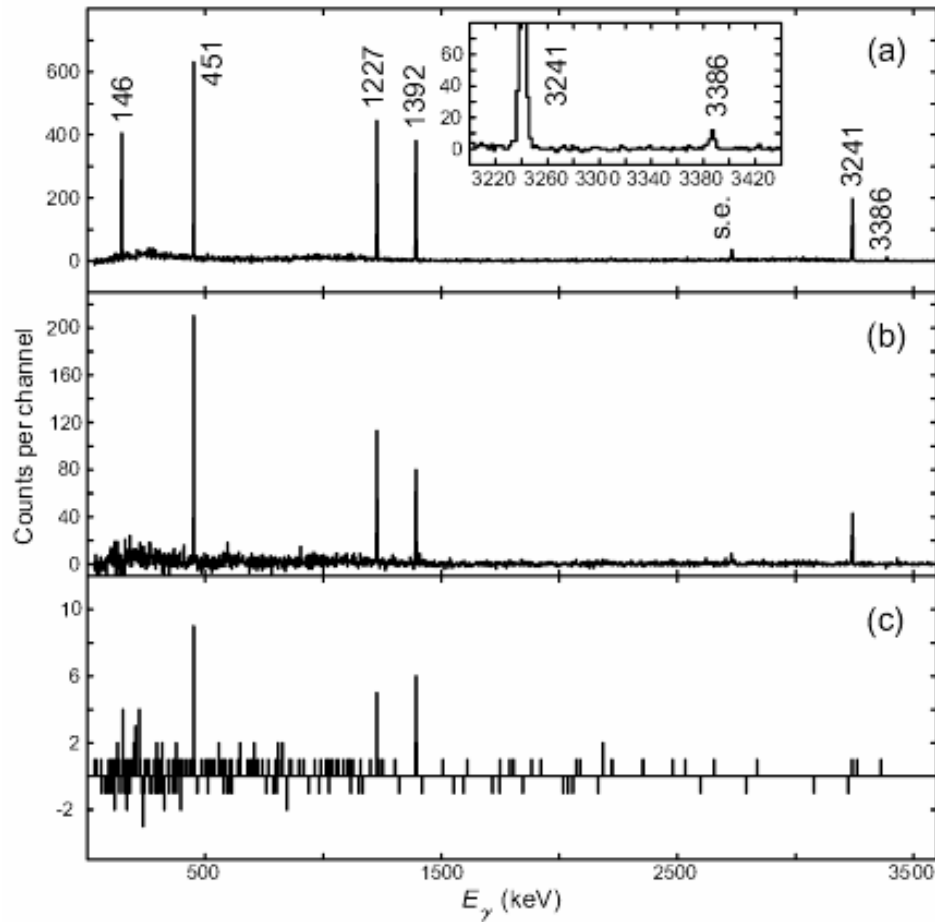


Figure 8.6: Three projections of a  $Z = 28$  gated  $\gamma - \gamma$  matrix for the time interval  $50 \text{ ns}$  to  $1.1 \mu\text{s}$ . All  $\gamma$  rays hitting the detector array in coincidence with one of the known transitions in  $^{54}\text{Ni}$  (451, 1227 or 1392 keV) are shown in (a). In (b) a gate has been placed on the 146 keV line to see all coincidences with this line. (c) is gated on the 3386 keV line to clearly show that it is part of the cascade. The low statistics is due to the very few counts in the gated peak, but the spectrum is unambiguous. The "s.e." marked peak is the single escape peak of the 3241 keV transition.

## 8.2 Discussion

The results of the preliminary data analysis meet our expectations, and reveal physics details beyond these. This section discusses in some more detail the implications of the presented graphs, projections, and matrices.

### The $^{54}\text{Ni}$ Cascade

From the level scheme of  $^{54}\text{Fe}$  [20], the  $^{54}\text{Ni}$  mirror nucleus, we would expect either five or six peaks to be visible: the  $E2$   $\gamma$  decay from the isomeric  $10^+$  state to the  $8^+$  level via a low energy  $\gamma$  ray (146 keV line), the  $E2$   $\gamma$  decay of the  $8^+$  state to the  $6^+$  state with a high energy  $\gamma$  ray (3241 keV line) and finally the previously identified [21]  $\gamma$  cascade (451 keV, 1227 keV, 1392 keV) down to the  $0^+$  ground state of  $^{54}\text{Ni}$ . Due to the small branching ratio and, hence, lack of intensity, the  $E4$  decay ( $10^+ \rightarrow 6^+$  transition) is not visible in the singles  $\gamma$  spectrum and thus, we should see five  $^{54}\text{Ni}$  transitions in Fig. 8.3.

To prove that these five candidates really are part of the  $^{54}\text{Ni}$  cascade down to the ground state, the  $\gamma - \gamma$  matrix projections in Fig. 8.6 are studied. As the projections of the matrix reveal all observed coincidences, and it makes use of the same  $Z = 28$  gate as the single  $\gamma$  spectrum in Fig. 8.3, all peaks visible must originate from the isomeric decay of Ni and be emitted more or less simultaneously. Comparing the singles  $\gamma$  spectrum with Fig. 8.6(a), there are three major changes visible in the  $\gamma - \gamma$  spectrum:

1. Neither the 741 keV line, nor the strong 1327 keV line is present, which indicates that neither of them are part of the  $^{54}\text{Ni}$  cascade. Both lines were identified as known transitions in *other* nuclei than  $^{54}\text{Ni}$ . The 741 keV line was unambiguously identified as a transition from the  $3/2^-$  excited state in  $^{53}\text{Fe}$  to its  $7/2^-$  ground state [2], having both the correct energy and half-life [ $T_{1/2}(\text{RISING}) = 92(2)$  ns;  $T_{1/2} = 91.6(20)$  ns]. The 1327 keV line was identified as a transition from the first excited  $9/2^-$  state in  $^{53}\text{Co}$  to its  $7/2^-$  ground state. These two lines will be discussed further below.
2. A small peak at 3386 keV emerges from the background. By recognising the fact that the sum of 146 keV and 3241 keV is very close to the energy of this observed transition, it is highly unlikely that it is anything other than the  $E4$  transition that has been "missing" in the single  $\gamma$  spectrum. Figure 8.6(c) shows the  $6^+ \rightarrow 4^+ \rightarrow 2^+ \rightarrow 0^+$  cascade, ensuring that the peak at 3386 keV is the  $10^+ \rightarrow 6^+$   $E4$  decay of the isomer.
3. A small "background" peak at 2730 keV is slightly enhanced. As the energy of this peak corresponds to 3241 keV minus 511 keV, it is the single escape peak.

A short table follows to summarise these results:

Table 8.1: Observed  $\gamma$ -rays.

| Nucleus          | Energy [keV] | Type | Transition                |
|------------------|--------------|------|---------------------------|
| $^{54}\text{Ni}$ | 146.2(2)     | $E2$ | $10^+ \rightarrow 8^+$    |
| $^{54}\text{Ni}$ | 451.1(2)     | $E2$ | $6^+ \rightarrow 4^+$     |
| $^{54}\text{Ni}$ | 1227.3(2)    | $E2$ | $4^+ \rightarrow 2^+$     |
| $^{54}\text{Ni}$ | 1392.2(2)    | $E2$ | $2^+ \rightarrow 0^+$     |
| $^{54}\text{Ni}$ | 3240.5(3)    | $E2$ | $8^+ \rightarrow 6^+$     |
| $^{54}\text{Ni}$ | 3386.3(5)    | $E4$ | $10^+ \rightarrow 6^+$    |
| $^{53}\text{Fe}$ | 741.1(2)     | $E2$ | $3/2^- \rightarrow 7/2^-$ |
| $^{53}\text{Co}$ | 1327.3(2)    | $M1$ | $9/2^- \rightarrow 7/2^-$ |

### Branching Ratio

As the different gates used in Fig. 8.6(b) and (c) further illustrate, the observed peaks are true coincidences. Now that the  $E4$  transition has been observed, the branching ratio can be determined by comparing the intensities of the  $E2$  and the  $E4$   $\gamma$  decay from the isomeric  $10^+$  state. Usually this cannot be done directly by dividing the number of counts in the respective peaks with the sum of their counts, because of the detector efficiency curve. For Ge-arrays like the one used, this curve flattens out considerably beyond 1500 keV, so that to first approximation the detector-array efficiency is the same at 3241 keV as at 3386 keV  $\gamma$  energy. Even though this is an incorrect way of calculating the branching ratio, in this case it yields a good enough approximation: 5.1(10)%  $E4$  : 94.9(10)%  $E2$ .

### The $^{53}\text{Co}$ Line

A very interesting observation in the spectra of Fig. 8.3 and Fig. 8.6 is the  $^{53}\text{Co}$  line. The spectra are  $Z = 28$  gated, and thus ensure that Ni is implanted. Except for  $^{54}\text{Ni}$ , two more Ni isotopes reached the S4 setup in the experiment:  $^{53}\text{Ni}$  and  $^{55}\text{Ni}$  – of which the trace amounts of  $^{53}\text{Ni}$  would not in any way be able to explain the high intensity of the observed peak, and  $^{55}\text{Ni}$  definitely showed no sign of a long-lived isomeric state. This is easily proven by specifically gating on the isotope in question. Another possible explanation could be secondary nuclear reactions in the S4 degrader, the Sc42 and the stopper, which all three are behind the particle identification. LISE++ simulations show that this is no reasonable explanation due to the too low ( $\sim 3$  orders of magnitude lower than required)  $^{53}\text{Co}$  yield.

Searching for explanations in the physics, a solution is quickly found. The difference between  $^{54}\text{Ni}$  and  $^{53}\text{Co}$  is one proton. While the ground state energy of the  $^{53}\text{Co}+p$ -system is higher than the ground state energy of  $^{54}\text{Ni}$ , the  $10^+$  isomer level lies some 2607 keV above the ground state of  $^{53}\text{Co}$  and 1277 keV above  $^{53}\text{Co}$ 's first excited state ( $9/2^-$ ). The solution to the problem is that one of the possible decay channels of the  $10^+$  isomer in  $^{54}\text{Ni}$  directly goes to the first excited state in  $^{53}\text{Co}$  via proton emission. Both Fig. 8.3 and Fig. 8.6 strongly suggest this solution as we have no coincidence of the 1327 keV line with the  $^{54}\text{Ni}$  cascade, but a strong overall intensity of this single  $\gamma$  peak.

Viewing the 1327 keV  $^{53}\text{Co}$  emission as another decay channel, the branching ratio is of the order of 40% of the total intensity. Yet one question remains: considering the proton-decay of the  $10^+$  isomer in  $^{54}\text{Ni}$  to the first excited state in  $^{53}\text{Co}$ , is there a direct decay channel to the ground state of  $^{53}\text{Co}$  as well? With the experimental data obtained in this experiment there is no way of answering this question, because we observe  $\gamma$  rays only and this decay channel would not emit any  $\gamma$  radiation. Another invisible candidate for a decay channel comprising the emission of protons would be a two-proton decay to  $^{52}\text{Fe}$ . The energy of the  $^{52}\text{Fe}+2p$ -system lies some 997 keV below the  $10^+$  isomer in  $^{54}\text{Ni}$ . However, if the intensity of the two-proton decay channel is comparable to that if the single proton emission is questionable.

### Level Scheme

To put all the above discussed transitions into context, Fig. 8.7 provides a level scheme of the  $^{54}\text{Ni}$  and  $^{53}\text{Co}$  transitions, which summaries the observed  $\gamma$  decays.

### Lifetime of the $10^+$ Isomer

As described in section 8.1, the lifetime of the Ni isomer was analysed by means of a least squares fit to a carefully chosen data interval. The from Fig. 8.5 obtained lifetime,  $1/\lambda$ , is 223 ns. The output error of the fit is of the order of approximately 3 ns, but fitting a slightly different time interval yields lifetimes that differ from the primary value. This fact requires the error to be extended to about 10 ns. The final value for the lifetime obtained by the mentioned methods in the preliminary data analysis is thus 223(10) ns.

### The $^{53}\text{Fe}$ Line and Other Mysteries

Issues that will require further investigations are first and foremost the 741 keV  $^{53}\text{Fe}$  line and the  $^{54}\text{Fe}$  lines that were observed in the singles  $\gamma$  spectrum in Fig. 8.3. Regarding the  $^{53}\text{Fe}$  line can be said that the mechanisms for the production of this nucleus after the particle identification can be basically ruled out as a possible explanation. Apparently, the cross sections for secondary reactions causing this are approximately four to five orders of magnitude too low for being an explanation. Currently we see no way of getting  $^{53}\text{Fe}$  as we implant  $Z = 28$  (Ni) ions into the stopper. Considering a possible physics explanation, one has to face one severe problem:  $^{53}\text{Fe}$  has one neutron more, and two protons less than  $^{54}\text{Ni}$ . The quickest natural way of making  $^{53}\text{Fe}$  out of  $^{54}\text{Ni}$  is to let the  $^{54}\text{Ni}$  isomer decay to  $^{53}\text{Co}$ , from where it should continue to  $^{53}\text{Fe}$  via either  $\beta^+$  decay or electron capture. The problem here is that the half-life of

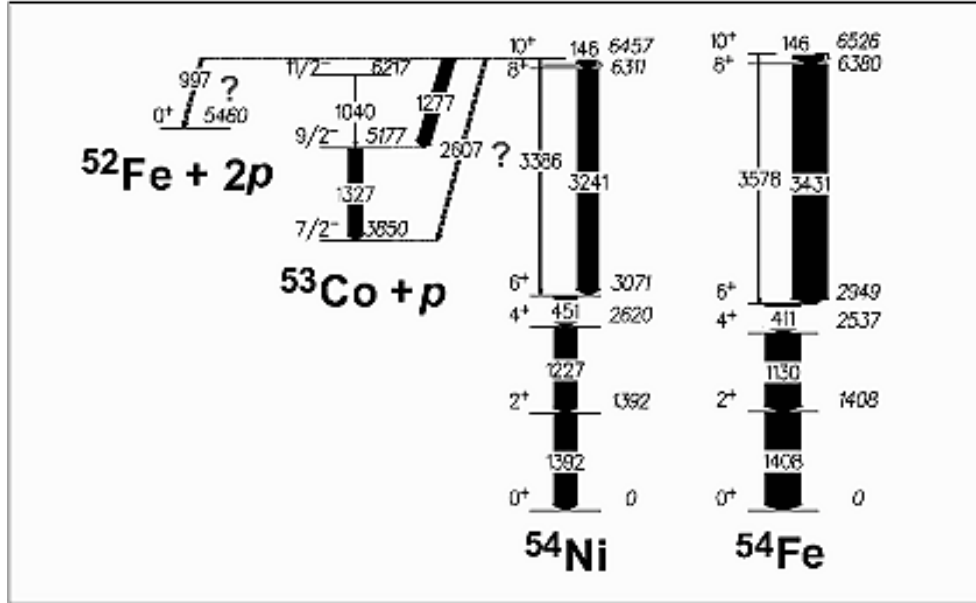


Figure 8.7: A level scheme that shows the connection between the observed  $\gamma$  decays. The level scheme of the  $^{54}\text{Ni}$  mirror nucleus  $^{54}\text{Fe}$  shows the striking similarities of the structure of these two nuclei.

$^{53}\text{Co}$  is 240 ms. Even if the  $\beta^+$  decay or electron capture could populate the  $3/2^-$  state in  $^{53}\text{Fe}$ , with this half-life the observed  $\gamma$ -rays should be seen as completely Ni independent and disappear once the background has been subtracted. This is *not* the case, as the 741 keV line is not present in the  $Z = 27$  gated singles  $\gamma$  spectrum.

The observed  $^{54}\text{Fe}$  lines also pose a riddle. In Fig. 8.3 these "background" lines had to be removed making use of the longer lifetime of the  $^{54}\text{Fe}$  isomer as compared to the  $^{54}\text{Ni}$  one. By creating a cut from  $0.58 \mu\text{s}$  to  $1.2 \mu\text{s}$ , scaling by an appropriate factor, and subtracting it from the Ni data, the lines were made to disappear. The question of where we get these lines from still remains.

Hopefully, the continued investigations on this matter will provide some answers in the near future.



## Chapter 9

# Conclusions and Outlook

The  $^{54}\text{Ni}$  experiment has been successfully prepared by means of MOCADI and LISE++ simulations. The experimental technique and the experimental setup worked flawlessly and yielded a good amount of high quality data. Preliminary data analysis has unambiguously identified the  $^{54}\text{Ni}$  cascade and an alternative decay channel, with about 40% of the overall decay probability, via isomeric proton decay to  $^{53}\text{Co}$ . The branching ratio between the  $E2$  and  $E4$  decay channel of the  $^{54}\text{Ni}$  isomer has been estimated to be 5.1(10)%  $E4$  : 94.9(10)%  $E2$ . The lifetime of the isomer has been estimated to be 223(10) ns, while more thorough future analysis will be able to improve the value and decrease its uncertainty.

Implications of the obtained results will be further investigated in future efforts, for example the in Chapter 2 mentioned mirror energy difference. This is a direct test of the existing models for the behaviour atomic nuclei. The in Fig. 9.1 plotted energy differences were obtained from

$$MED_I = E_I(^{54}\text{Ni}) - E_I(^{54}\text{Fe}),$$

where  $I$  signifies the nuclear spin of the respective energy level. These latest results extend those presented in [21].

The observation of isomeric proton decay in the  $^{54}\text{Ni}$  experiment has caught our interest, as this is a phenomenon rarely observed. In November 2006, the next step in our proton decay investigations will be a challenging experiment held in Cologne, Germany, dedicated to measuring the protons directly. If this experiment turns out to be a success, we would be the first to directly observe this type of decay. Hopefully, this experiment will yield as many unexpected and interesting results as the stopped beam  $^{54}\text{Ni}$  experiment.

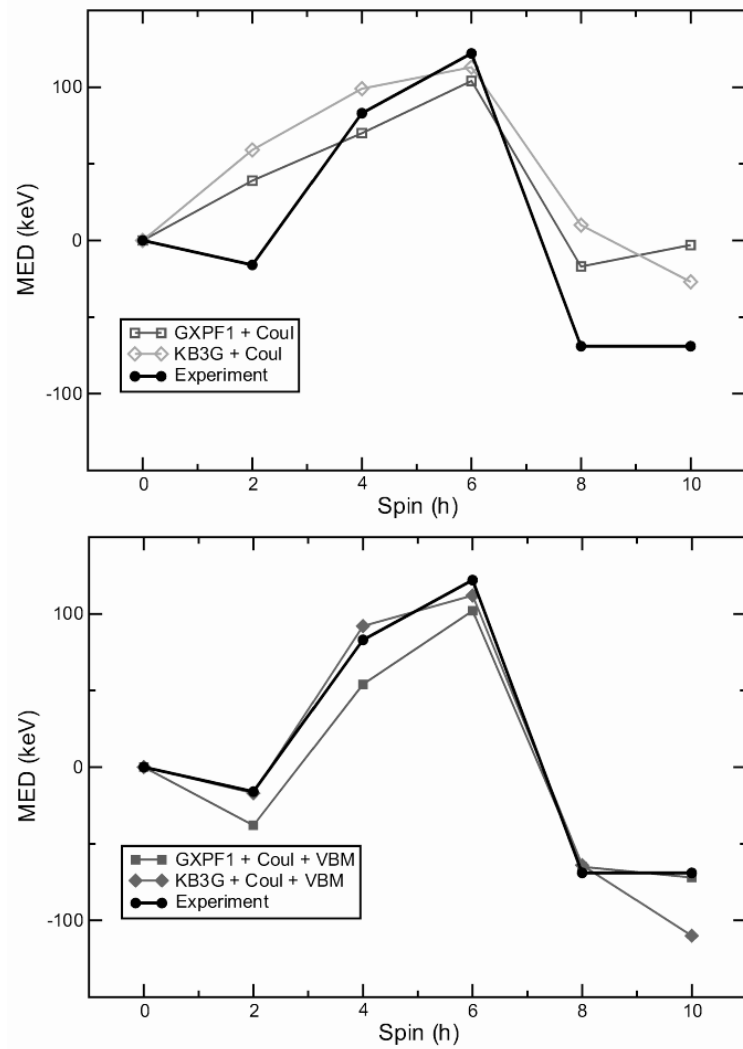


Figure 9.1: The figure shows a Mirror Energy Difference (MED) plot for the two  $A = 54$  nuclei  $^{54}\text{Ni}$  and  $^{54}\text{Fe}$ . Predictions of different calculation models are compared with the results of the experiment, which extends the available MED data on these nuclei to a nuclear spin of  $I = 10$ . The lower of the two figures shows the results of calculations that include an isospin breaking component in the strong force.



## Chapter 10

# Populärvetenskaplig Sammanfattning

Kärnfysiken är ett aktivt och dynamiskt forskningsområde som ständigt vidareutvecklas. Denna forskning har lett till stora framsteg inom för samhället essentiella områden som till exempel energiteknik och medicin. Våra modeller för hur atomkärnor beter sig under olika omständigheter är långt ifrån att vara kompletta. Experimentet och dess resultat som detta examensarbete handlar om, är ännu en viktig pusselbit i förståelsen av samspelet mellan nukleoner, dvs. protoner och neutroner.

Experimentets mål är att undersöka kärnstrukturen i den kortlivade radioaktiva nickelisotopen  $^{54}\text{Ni}$ , som man hittills inte visste mycket om. Denna kärna är av intresse då man vill studera hur den starka kraften, som håller ihop atomkärnor och till första approximation inte bryr sig om elektisk laddning, skiljer mellan de positivt laddade protonerna och de neutralt laddade neutronerna i kärnan. En sådan undersökning kan göras med hjälp av så kallade spegelkärnor – par av atomkärnor med samma totala antal nukleoner, men med speglade proton- och neutrontal: spegelkärnan till  $^{54}_{28}\text{Ni}_{26}$  är den välstuderade stabila kärnan  $^{54}_{26}\text{Fe}_{28}$ .

I arbetet beskriver jag den experimentella metoden som används för studien av  $^{54}\text{Ni}$ , den inblandade utrustningen och tillvägagångssättet. Fokus av arbetet är förberedelserna i form av datorsimuleringar som måste göras innan själva experimentet. Inte enbart resultaten av dessa förberedelser presenteras, utan även en komplett guide som i detalj beskriver hur man använder simuleringsprogrammen som finns. Själva experimentet beskrivs kortfattat och en sammanfattning och diskussion av de preliminära resultaten avslutar arbetet.

I  $^{54}\text{Ni}$  observerades en så kallad isomer, ett långlivat högre energitillstånd i en atomkärna. När kärnan slutligen faller tillbaka till sitt grundtillstånd som har lägre energi, avslöjas kärnans struktur genom utsändandet av gammastrålning. Under experimentet observerar vi denna strålning och kan därmed rekonstruera strukturen hos  $^{54}\text{Ni}$ . Det observerades även ett något oväntat fenomen: det högre energitillståndet i  $^{54}\text{Ni}$  sönderföll inte enbart via gammasönderfall, utan kunde även direkt från det långlivade tillståndet sönderfalla till  $^{53}\text{Co}$  genom att sända ut en proton.

$^{54}\text{Ni}$  experimentet var ett av tre mycket framgångsrika experiment i en pågående forskningskampanj som kommer att leda till ökad förståelse om hur naturen egentligen fungerar på subatomär nivå.

# Chapter 11

## Acknowledgments

First and foremost, I would like to thank my supervisor, and friendly soul, Dr. Dirk Rudolph for giving me the unique opportunity to jump-start into the realm of nuclear structure physics research. Also, I want to remark the much appreciated feedback he provided whenever I needed it. He also gets credit for vigorously taking care of large parts of the preliminary data analysis.

Special thanks to Prof. Claes Fahlander and the whole Nuclear Structure Group who welcomed and treated me as one of them right from the start. Very special thanks to Dr. Margareta "Maggie" Hellström, for her constant guidance and sharing her expertise – without her, things would have been much more difficult and certainly less successful.

Also, I would like to thank all my crazy buddies and students at the Fysicum here in Lund, for providing the stimulating environment this place is known for. Last but not least, I would like to thank my family for supporting me throughout the years of my studies.

May the  $m \cdot a$  be with you all... always.



# Bibliography

- [1] J. Ekman, Ph. D. Thesis, Lund University, 2004, ISBN 91-628-6061-5.
- [2] R. du Rietz, Ph. D. Thesis, Lund University, 2005, ISBN 91-628-6394-0.
- [3] M.N. Mineva, Ph. D. Thesis, Lund University, 2004, ISBN 91-628-6143-3.
- [4] R. Serber, Phys. Rev. 72, 1114 (1947).
- [5] B. Blank *et al.*, Phys. Rev. C 50, 2398 (1994).
- [6] K. Sümmerer *et al.*, Phys. Rev. C 42, 2546 (1990).  
EPAX 2.1, <http://www-w2k.gsi.de/hellstr/asp/gsi/epaxv21m.asp>
- [7] Schmidt-Ott *et al.*, Z.Phys. A 350, 215 (1994).
- [8] H. Geissel *et al.*, NIM B70 286-297 (1992).
- [9] Bethe-Bloch Formula, From Wikipedia  
[http://en.wikipedia.org/wiki/Bethe-Bloch\\_formula](http://en.wikipedia.org/wiki/Bethe-Bloch_formula)
- [10] The available FRS Targets,  
<http://www-w2k.gsi.de/kindler/frs/FRS-HTML/CS-PL.htm>
- [11] Degradation settings and characteristics,  
<http://www-w2k.gsi.de/frs-Setup/Degradation%20Settings.htm>
- [12] Pascale Mayet, Ph. D. Thesis, GSI Darmstadt, 2000.
- [13] On the function and construction of MWPCs at the FRS,  
<http://www-linux.gsi.de/~weick/frs/mwpc.html>
- [14] EUROBALL III, A European  $\gamma$ -ray facility, Eds. J. Gerl and R.M. Lieder, GSI 1992.
- [15] J.-J. Gaimard and K.-H. Schmidt, Nucl. Phys. A531, 709 (1991).  
MOCADI Homepage, H. Weick, N. Iwasa *et al.*, 2005.  
<http://www-linux.gsi.de/~weick/mocadi/>
- [16] D. Bazin, O. Tarasov *et al.*, NIM A 482 (2002) 307.  
O. Tarasov, D. Bazin, Nuclear Physics A 746 (2004) 411.  
<http://dnr080.jinr.ru/lise/lise.html>

- [17] Example input file, <http://wwwnsg.nuclear.lu.se/personal/hoischen/>
- [18] Physics Analysis Workstation homepage, <http://paw.web.cern.ch/paw/>
- [19] The ROOT homepage, <http://root.cern.ch/>
- [20] Nuclear Data Services, <http://www-nds.iaea.org/>
- [21] A. Gadea *et al.*, to be submitted.